AEDC-TR-71-215

cy 2

JAN 13 1972
FEB 9 1972

THREE-DIMENSIONAL LAMINAR BOUNDARY-LAYER ANALYSIS OF UPWASH PATTERNS AND ENTRAINED VORTEX FORMATION ON SHARP CONES AT ANGLE OF ATTACK

John C. Adams, Jr.

ARO, Inc.

December 1971

Approved for public release; distribution unlimited.

VON KÁRMÁN GAS DYNAMICS FACILITY
ARNOLD ENGINEERING DEVELOPMENT CENTER
AIR FORCE SYSTEMS COMMAND
ARNOLD AIR FORCE STATION, TENNESSEE

PROPERTY OF U S AIR FORCE
AEDC LIBRARY
F40600-72-C-0003

NOTICES

When U. S. Government drawings specifications, or other data are used for any purpose other than a definitely related Government procurement operation, the Government thereby incurs no responsibility nor any obligation whatsoever, and the fact that the Government may have formulated, furnished, or in any way supplied the said drawings, specifications, or other data, is not to be regarded by implication or otherwise, or in any manner licensing the holder or any other person or corporation, or conveying any rights or permission to manufacture, use, or sell any patented invention that may in any way be related thereto.

Qualified users may obtain copies of this report from the Defense Documentation Center.

References to named commercial products in this report are not to be considered in any sense as an endorsement of the product by the United States Air Force or the Government.

THREE-DIMENSIONAL LAMINAR BOUNDARY-LAYER ANALYSIS OF UPWASH PATTERNS AND ENTRAINED VORTEX FORMATION ON SHARP CONES AT ANGLE OF ATTACK

John C. Adams, Jr.
ARO, Inc.

Approved for public release; distribution unlimited.

FOREWORD

The work reported herein was sponsored by Headquarters, Arnold Engineering Development Center (AEDC), Air Force Systems Command (AFSC), under Program Element 64719F.

The results of research presented were obtained by ARO, Inc. (a subsidiary of Sverdrup & Parcel and Associates, Inc.), contract operator of AEDC, AFSC, Arnold Air Force Station, Tennessee, under Contract F40600-72-C-0003. The research was conducted from July, 1970, until May, 1971, under ARO Project No. VW5106, and the manuscript was submitted for publication on July 21, 1971.

The author wishes to thank Mr. John B. McDevitt, Research Scientist, NASA Ames Research Center, Moffett Field, California, for providing the author with copies of the original photographs from his oil-flow studies. Acknowledgement and appreciation is also extended to Dr. R. T. Davis, Professor of Engineering Mechanics, Virginia Polytechnic Institute and State University, Blacksburg, Virginia, for providing the author with a copy of his three-dimensional laminar boundary-layer digital computer program. In the course of the present work many stimulating discussions were held with Mr. Sam R. Pate, Supervisor, Impulse Tunnels Section, Aerodynamics Projects Branch, Aerodynamics Division, von Kármán Gas Dynamics Facility, ARO, Inc., concerning the meaning and correct application of the maximum crossflow Reynolds number concept for hypersonic flows.

This technical report has been reviewed and is approved.

Maurice A. Clermont
Captain, CF
Research & Development Division
Directorate of Technology

Robert O. Dietz
Acting Director
Directorate of Technology

ABSTRACT

Application of three-dimensional inviscid and viscous (laminar boundary layer) analyses for cold wall hypersonic flows over sharp cones at incidence is presented relative to experimental data, showing surface upwash angles and entrained vortex formation leading to crossflow-induced boundary-layer transition. Three-dimensional neutral inviscid stability theory for stationary disturbances is used to calculate the angular orientation of the entrained vortices in the boundary layer while a maximum crossflow Reynolds number concept is applied for correlation of the onset to vortex formation due to crossflow instability. In general, excellent agreement between boundary-layer theory and experiment is obtained relative to surface upwash angles. The inviscid stability theory yields reasonable estimates for the vortex angular orientation while the correlation of distance to onset of vortex formation by a critical maximum crossflow Reynolds number concept is in good agreement with previous investigations on swept cylinders and wings under subsonic and supersonic conditions. The calculated surface upwash angle and maximum crossflow Reynolds number are found to be sensitive to wall temperature effects with the larger values of the angle or crossflow Reynolds number occurring with the hotter wall.

CONTENTS

Page

ABSTRACT iii
NOMENCLATURE vi
I. INTRODUCTION 1
II. ENTRAINED VORTEX FORMATION IN THE LAMINAR BOUNDARY LAYER
2.1 Formation of Entrained Vortices and Their Relationship with the Cross-Hatching Phenomenon 3
2.2 Three-Dimensional Boundary-Layer Stability Theory 5
2.3 Correlation of Distance to Onset of Vortex Formation in the Three-Dimensional Laminar Boundary Layer 9
III. ANALYTICAL ANALYSIS
3.1 Inviscid Flow 10
3.2 Viscous Boundary-Layer Flow 11
IV. BODY AND FLOW CONDITIONS 12
V. RESULTS AND DISCUSSION 13
VI. CONCLUDING SUMMARY 17
REFERENCES 19

APPENDIXES

I. ILLUSTRATIONS

Figure

1. Three-Dimensional Boundary-Layer Velocity Profiles in Streamline Coordinates 27
2. Schematic of Disturbance Wave Propagation in a Three-Dimensional Boundary Layer 28
3. Sharp Cone Geometry and Nomenclature 29
4. Schematic of Three-Dimensional Boundary-Layer Velocity Profile in Body Coordinates Showing Definition of Upwash Angles 30
5. Calculated Upwash Angles for Sharp Cones in Inviscid Flow 31
6. Comparison of Calculated and Measured Surface Upwash Angles 34
7. Effects of Wall Temperature on Calculated Surface Upwash Angle 37
8. Variation of Surface Upwash Angle with Wall Temperature at a Given Circumferential Location 38
9. Comparison of Calculated and Measured Vortex Angles at the Body Location ϕ = 90 deg 39
10. Angular Turning of the Boundary-Layer Velocity Profile at the Body Location ϕ = 90 deg Including Position of Critical Height 41
11. Maximum Crossflow Reynolds Number Distribution 42
12. Developed-Surface Plot Showing Onset to Vortex Formation Relative to Lines of Constant Maximum Crossflow Reynolds Number 43

Figure | Page

13. Effects of Wall Temperature on Calculated Maximum Crossflow Reynolds Number Distribution 45
14. Effects of Wall Temperature on Maximum Crossflow Velocity in Boundary Layer 46
15. Effects of Wall Temperature on Boundary-Layer Thickness 47

II. TABLES

I. Laminar Three-Dimensional Boundary-Layer Profiles at ϕ = 90 deg for δ_v = 10 deg and α = 5 deg 48
II. Laminar Three-Dimensional Boundary-Layer Profiles at ϕ = 90 deg for δ_v = 10 deg and α = 6 deg 49
III. Laminar Three-Dimensional Boundary-Layer Profiles at ϕ = 90 deg for δ_v = 10 deg and α = 8 deg 50
IV. Laminar Three-Dimensional Boundary-Layer Profiles at ϕ = 90 deg for δ_v = 15 deg and α = 5 deg 51

NOMENCLATURE

A	Composite stability parameter from Eq. (45) in Reshotko (Ref. 37)
A_c	Critical value of composite stability parameter
c	Disturbance propagation velocity
c_i	Imaginary part of disturbance propagation velocity
c_r	Real part of disturbance propagation velocity
F	Fluctuating quantity
f	Amplitude of fluctuating quantity
L	Slant length of sharp cone
M_∞	Free-stream Mach number
p_e	Static pressure at outer edge of boundary layer
p_∞	Free-stream static pressure
R	Specific gas constant for air, 1716 $ft^2/sec^2\text{-}^\circ R$
Re_{ref}	Reference Reynolds number from Eq. (35) in Reshotko (Ref. 37)

$Re_{\infty,L}$	Free-stream Reynolds number, $\rho_\infty V_\infty L/\mu_\infty$
T	Static temperature
T_e	Static temperature at outer edge of boundary layer
T_o	Stagnation temperature
T_w	Wall temperature
$\overline{T}$	Static temperature ratio, T/T_e
$\overline{T}_c$	Critical value of static temperature ratio, T_c/T_e
t	Time
U_e	Streamwise velocity component at outer edge of boundary layer
u	Streamwise velocity component
$\overline{u}$	Streamwise velocity component ratio, u/U_e
$\overline{u}_c$	Critical value of streamwise velocity component ratio, u_c/U_e
V_∞	Free-stream velocity
v	Normal velocity component
W_e	Crossflow velocity component at outer edge of boundary layer
$\overline{W}$	Composite dimensionless velocity from Eq. (24) in Reshotko (Ref. 37)
w	Crossflow velocity component
$w_{s\ell,max}$	Maximum value of crossflow velocity component in streamline coordinate system
$\overline{w}$	Crossflow velocity component ratio, w/W_e
$\overline{w}_c$	Critical value of crossflow velocity component ratio, w_c/W_e
x	Coordinate along body surface in streamwise velocity direction
$x_{s\ell}$	Coordinate along body surface in outer edge streamline direction
$y, y_{s\ell}$	Coordinate normal to body surface

y_c	Critical height
z	Coordinate along body surface in crossflow velocity direction
$z_{s\ell}$	Coordinate along body surface perpendicular to outer edge streamline direction
α	Angle of attack
α_d	Disturbance wave number, $2\pi/\lambda$
γ	Ratio of specific heats, 1.40
δ	Boundary-layer thickness
δ_v	Sharp cone semivertex angle
ϵ_i	Inviscid surface upwash angle
ϵ_s	Surface upwash angle
ϵ_v	Vortex angle
θ	Angle of wave propagation direction relative to x-axis
θ_c	Critical angle of wave propagation direction relative to x-axis
λ	Disturbance wavelength
μ_e	Viscosity at outer edge of boundary layer
μ_∞	Free-stream viscosity
π	Pi, 3.14159
ρ_e	Density at outer edge of boundary layer
ρ_∞	Free-stream density
ϕ	Circumferential body surface coordinate
χ_{max}	Maximum crossflow Reynolds number, $\rho_e w_{s\ell,max}\delta/\mu_e$
ψ	Angle between resultant external velocity and x-axis

SUBSCRIPTS

c	At critical height, y_c
d	Disturbance
e	Outer edge of boundary layer
i	Imaginary part; inviscid
L	Based on slant length of sharp cone
max	Maximum value
o	Total or stagnation
r	Real part
ref	Reference value
s	Surface
$s\ell$	Streamline coordinate system
v	Vortex
w	Wall
∞	Free-stream condition

SUPERSCRIPTS

$'$	Derivative with respect to y
$-$	Nondimensional quantity

SECTION I
INTRODUCTION

The laminar boundary layer on a sharp cone at incidence is of practical importance in several applications, such as high-speed aircraft and lifting reentry vehicles. For lifting reentry in particular, a knowledge of the full three-dimensional boundary-layer properties is essential for accurately estimating the local heat-transfer and skin-friction distributions around the vehicle, including the determination of separated flow regions. In addition, information yielding the surface streamline direction of the three-dimensional boundary-layer flow is needed in order to ascertain boundary-layer influence on vehicle control surfaces.

Existing flight test data and recent ground test data (Refs. 1, 2, 3, and 4) have indicated that boundary-layer transition, as well as spatial distribution of the transition front, can have significant effect on the aerodynamic behavior of slender conical reentry bodies at incidence. Under certain free-stream conditions for hypersonic flow over a sharp cone at incidence, transition from laminar to turbulent boundary-layer flow follows the spatial distribution shown below taken from Ref. 4 for a 7.2-deg, half-angle sharp cone at free-stream Mach number eight and cold wall conditions.

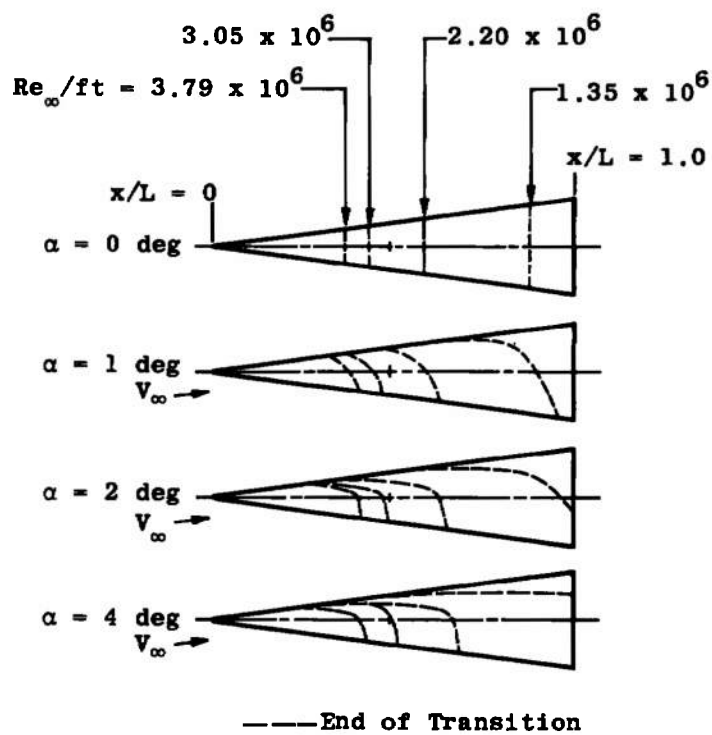

In general, with increasing angle of attack the above-indicated transition movement undergoes a much more rapid forward progression on the leeward side than the rearward progression for the windward side. However, under other free-stream conditions, onset

to transition does not occur along the windward ray as indicated above but begins at some angular location off the windward ray with the appearance of streamwise-directed vortices entrained within the boundary layer (see Ref. 5 for excellent photographic documentation of this phenomenon based on hypersonic wind tunnel tests of a nonablating sharp cone at incidence). Additional results from Ref. 5 concerning wind tunnel tests of ammonium-chloride ablating cones clearly reveal upwash groove patterns eroded in the model surface. These results were interpreted in Ref. 5 to be the result of vortices intensifying local heating rates which, as the work by Persen (Refs. 6 and 7) clearly shows, is certainly plausible. The upward inclination of the grooves on the ablating cones agreed closely with the inclination of the vortex paths measured on the nonablating cones using an oil-film technique under similar test conditions. Furthermore, the upward inclination of the vortices was considerably less than the inclination of surface streamlines in laminar flow but somewhat greater than the calculated inviscid upwash angle at the outer edge of the boundary layer. The important point to be gained from the above discussion of experimental results is that entrained vortices are formed under certain conditions in the three-dimensional laminar boundary layer on a sharp cone at incidence in a hypersonic flow under cold wall conditions. This vortex formation apparently signals the onset to three-dimensional crossflow-induced transition of the boundary layer from laminar to turbulent flow. It should be pointed out that this entrained vortex phenomenon is not limited to sharp cone flows but has been observed on spherically blunted cones as well (see Ref. 8).

In order to gain some insight into the physical processes causing vortex formation and crossflow-induced boundary-layer transition, an accurate knowledge of the influence of crossflow effects on the three-dimensional laminar boundary layer is essential. The mathematical theory of the three-dimensional laminar boundary layer as formulated by Moore (Ref. 9) and Hayes (Ref. 10) has been available for about twenty years. Only within the past four years, however, have accurate numerical integration techniques utilizing high-speed, large-memory digital computers become readily available for application to the three-dimensional boundary-layer problem. The reader is referred to the works of Der and Raetz (Ref. 11), Cooke (Ref. 12), Hall (Ref. 13), Powers, Niemann, and Der (Ref. 14), Der (Ref. 15), Dwyer (Refs. 16 and 17), Dwyer and McCroskey (Ref. 18), Krause (Ref. 19), Krause, Hirschel, and Bothmann (Refs. 20, 21, and 22), Boericke (Ref. 23), Vvedenskaya (Ref. 24), and McGowan and Davis (Ref. 25) for further study concerning the available analysis techniques for the complete three-dimensional laminar boundary-layer equations.

The present report will be devoted to application of three-dimensional inviscid and laminar viscous analyses for cold wall hypersonic flows over sharp cones at incidence, and comparison with experimental data that show upwash angles and entrained vortex formation leading to crossflow-induced boundary-layer transition. Three-dimensional neutral inviscid stability theory for stationary disturbances is used to calculate the angular orientation of the entrained vortices within the boundary layer in conjunction with application of a critical maximum crossflow Reynolds number concept for correlation of the onset to vortex formation due to crossflow instability. Effects of wall temperature on surface upwash angles and maximum crossflow Reynolds numbers are presented relative to ground testing of slender cones at incidence under hot wall conditions in hypersonic wind tunnels.

SECTION II
ENTRAINED VORTEX FORMATION IN THE LAMINAR BOUNDARY LAYER

The present study is devoted to analysis of experimental measurements revealing formation of entrained vortices in the three-dimensional laminar boundary layers on sharp cones at incidence in hypersonic flow. In order to understand physically how and when these entrained vortices appear in the laminar boundary layer, the present section is devoted to:

1. Review of recent literature on the cross-hatching phenomenon since the formation of entrained vortices in the boundary layer apparently is connected with the origin of cross-hatching.

2. Formulation of three-dimensional neutral inviscid stability theory for stationary disturbances with application to the calculation of angular direction for stationary vortex orientation in the boundary layer.

3. Application of the critical maximum local crossflow Reynolds number concept to the correlation of onset to vortex formation in the three-dimensional laminar boundary layer.

2.1 FORMATION OF ENTRAINED VORTICES AND THEIR RELATIONSHIP WITH THE CROSS-HATCHING PHENOMENON

The appearance of streamwise vortices entrained in the laminar boundary layer as discussed in Section I is not a new phenomenon but is, in fact, well-known and well-documented with respect to the cross-hatching problem. Wilkins (Ref. 26) and Wilkins and Tauber (Ref. 27) noted the formation of streamwise directed grooves in the surface of recovered models from ballistic-range tests. Larson and Mateer (Ref. 28) showed that the cross-hatching process appeared to originate at or just after the end of boundary-layer transition in a supersonic flow. Whether ablation itself was a necessary condition for cross-hatching or merely a means of recording the event could not be determined. The paper by Canning, Tauber, Wilkins, and Chapman (Ref. 29) cites experimental evidence for the presence of arrays of stationary vortices, and it is conjectured that the presence of these vortices may be connected with the origin of cross-hatching. Furthermore, the cross-hatch spiral angle is shown to correlate well with the boundary-layer edge Mach angle up to an edge Mach number of approximately two. For higher edge Mach numbers the cross-hatch spiral angle is greater than the edge Mach angle, suggesting that the disturbance causing the standing-wave system responsible for the cross-hatching can be near the edge or deeper within the boundary layer as the edge Mach number increases. The extensive study by Laganelli and Nestler (Ref. 30) using wind tunnel and rocket exhaust models constructed from various materials (Teflon®, phenolic nylon, carbon phenolic, and wood) as well as recovered flight vehicles shows clearly that the cross-hatching pattern phenomenon is not limited to melting ablators but also occurs in charring and subliming materials. In general, the experimental evidence indicates that the formation of cross-hatched patterns requires a supersonic turbulent boundary layer, and can be promoted by longitudinal grooving, surface roughness, and mass addition.

Based on the above-discussed experimental results, Tobak (Ref. 31) has postulated a hypothesis for the origin of cross-hatching based on the presence of an array of stationary vortices entrained within the boundary layer which, in turn, implies the presence of standing waves capable of producing the cross-hatch patterns. His hypothesis may be summarized as follows: Cross-hatching is the result of spatially periodic variations in surface pressure in both the spanwise and longitudinal directions. The source of the pressure variations is the presence within the boundary layer of an array of regularly spaced counterrotating stationary vortices. These vortices originate from surface irregularities near the leading edge of the body; the probability of their appearance is enhanced by the existence of small amounts of concave curvature of the boundary-layer streamlines. Surface ablation is not a necessary condition for the presence of the pressure variations that lead to cross-hatching, but may serve as the mechanism causing the streamline curvature and as a means of reinforcing and spreading the cross-hatch pattern once it appears.

The key point in all of the above is the formation of stationary vortices within the boundary layer. Persen (Ref. 32) has compiled an excellent survey of experimental evidence of the appearance of streamwise-directed vortices in fluid flow. Most experiments aimed at visualizing the streamwise vortices are in one way or another relying on an effect schematically exhibited below.

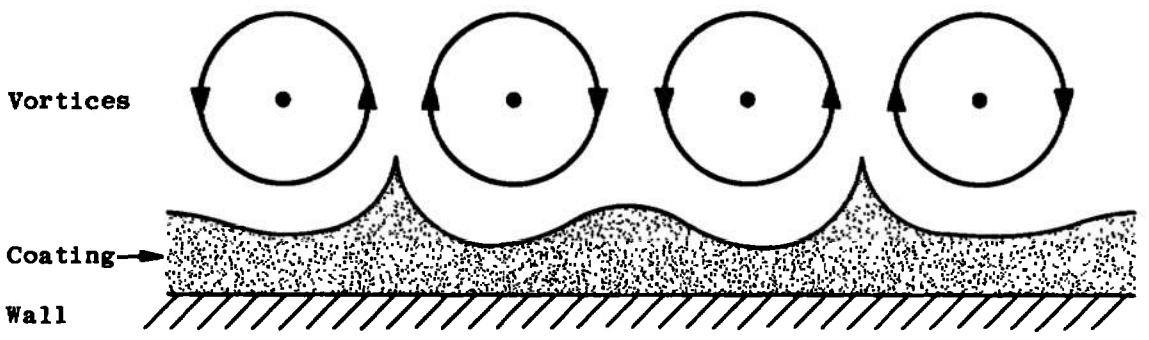

The oil-flow technique, such as used by McDevitt and Mellenthin (Ref. 5), is based on the principle that liquids coated on the surface of a body in a flow field will move in the same way as the fluid flow at the surface. In use of this technique, built-up ridges in the manner schematically indicated above represent evidence that streamwise directed vortices are present in the flow. As discussed by Persen (Ref. 32) the following features of the vortex system must be considered as experimentally proven:

1. The sidewise location of each vortex is fixed and exhibits a remarkable stability in the region where they are pronounced.

2. The vortex system breaks up further downstream. Two conclusions can be drawn from this observation:

    a. The vortex characteristics must be a function of the streamwise coordinate, and the changes which appear with increasing distance

must be such that the vortex becomes unstable and breaks down introducing a highly irregular motion (turbulence).

b. The vortex system seems to be in an intermediate state which, in view of stability theory, is introduced between a laminar motion upstream and the turbulent motion downstream.

3. In the two-dimensional cases the vortices seem to be confined into "boxes" of constant width λ in the crosswise direction to the main flow direction which is sometimes referred to as a "selective wavelength". The height of these "boxes" is a function of the streamwise coordinate.

4. The wavelength λ does not depend on the type of disturbance which may have initiated the creation of the vortex system. The wavelength is probably determined by a stability condition.

For the purposes of the current investigation the important point from the above discussion is simply that the origin of the vortex system seems to be directly related to the onset of transition in the boundary layer.

2.2 THREE-DIMENSIONAL BOUNDARY-LAYER STABILITY THEORY

Boundary-layer stability theory cannot currently be used to predict either the nonlinear details of the boundary-layer transition process or the location of transition onset. Stability theory can, however, establish which laminar boundary-layer profiles are unstable and the initial amplification rates of specific critical frequencies. A good and current review of the analytical methods used to attempt prediction of the location of transition from stability theory is presented by Jaffe, Okamura, and Smith (Ref. 33). However, it is to be emphasized that a thorough study of the connection between stability and transition still remains to be completed. For the reader interested in general study of modern boundary-layer stability theory using digital computer techniques, the author highly recommends the excellent comprehensive survey by Mack (Ref. 34). For an overview of the complete stability problem with emphasis on hypersonically traveling bodies, see the recent report by Morkovin (Ref. 35).

With respect to three-dimensional boundary-layer stability theory, the three-dimensional nature of the boundary-layer velocity profiles plays a crucial role. Referring to Fig. 1 (Appendix I), the velocity vector at a position $x_{s\ell}$, $z_{s\ell}$ of the surface is seen to twist out of the plane defined by the normal direction $y_{s\ell}$ and by the outer streamline, i.e., by the $x_{s\ell}$-direction. With the aid of the decomposition of the twisted vector family on the streamwise $x_{s\ell}$-$y_{s\ell}$ tangential plane and the $y_{s\ell}$-$z_{s\ell}$ crossflow plane, one can begin to visualize the three-dimensional vorticity distribution which ultimately feeds the unstable vorticity disturbances and which may be thought of as a superposition of Fourier components of all orientations for the disturbances at the given point $x_{s\ell}$, $z_{s\ell}$. However, as one proceeds to the neighboring points the local orientation of the wavefront may change because of nonuniformity of the crossflow. In other words, from a global view, the wavefronts of a given family may be curved. One should examine the

eigenvalue problem and local amplification rates in all these possible directions and find that direction in which the profile is first unstable and that in which it has maximum amplification at a higher Reynolds number. The wave disturbances with the front parallel to the $z_s\ell$-axis in Fig. 1 correspond to the normal two-dimensional Tollmien-Schlichting waves with their viscosity-induced relatively low amplifications. The wave disturbances with a wavefront along the $x_s\ell$-axis are primarily sensitive to the crossflow velocity profile $w_s\ell$. Figure 1 shows that this profile has a point of inflection indicating the possibility of a more rapid inviscid amplification along that direction (see Section III-2 of Ref. 35 for clarification).

In Part II of the paper by Gregory, Stuart, and Walker (Ref. 36), Stuart shows that the presence of these inflection points makes possible a meaningful simplification of the governing stability equations, namely the inviscid approximation. He singles out a plane rotated past the crossflow plane of Fig. 1 in which the point of inflection of the rotated velocity profile coincides with the $y_s\ell$-axis in Fig. 1, i.e., has zero velocity with respect to the wall at a height y_c as illustrated schematically below.

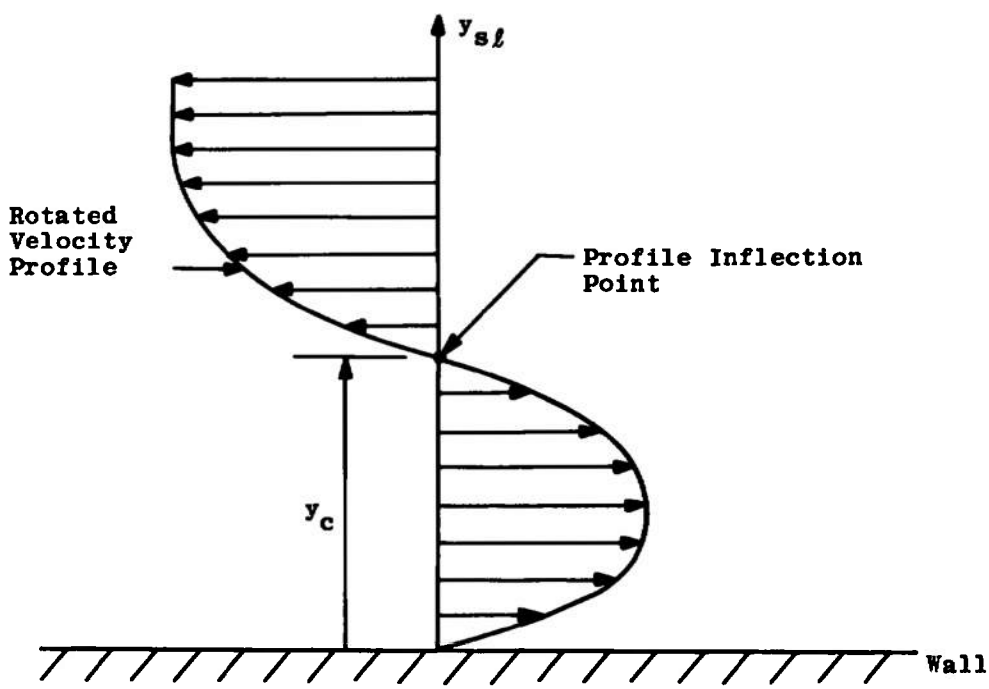

Roughly, amplification of that family of waves corresponds to an increasing concentration of vorticity oriented perpendicularly to that special plane at a height y_c. Because of the vanishing relative velocity, this vorticity concentration will form a stationary wave and can be made visible by sublimation, oil-flow, or smoke techniques. It is this type stationary wave which is observed as streaks in the oil-flow results of Ref. 5 and the china-clay results of Ref. 36.

The theoretical background for stability analysis of three-dimensional compressible boundary layers has been formulated by Reshotko (Ref. 37) based on his earlier analysis (Ref. 38) of the two-dimensional compressible boundary-layer stability characteristics. For Reynolds numbers sufficiently large that the dissipation terms in the disturbance energy equation are negligible, the stability of a three-dimensional boundary layer to a plane-wave disturbance of arbitrary orientation is shown to reduce to a two-dimensional stability problem governed by the boundary-layer velocity profile in the direction of wave propagation and by the mean temperature profile.

As discussed in Section III of Ref. 38, the governing disturbance equations of boundary-layer stability theory are regular everywhere except in the limit $y_s \ell \to \infty$, and the solutions of these equations are analytic functions of α_d (wave number of the disturbance), c (propagation velocity of the disturbance), and a Reynolds number Re_{ref} based on a reference length for all finite values of these parameters. The quantity $(\alpha_d\ Re_{ref})^{-1}$ appears in the disturbance equations as a parameter multiplying the highest order derivatives, and hence the method of asymptotic expansions valid for $(\alpha_d\ Re_{ref}) \gg 1$ may be applied by division of the disturbances into slowly varying solutions that are largely inviscid across the entire flow and "viscous" rapidly varying functions near the surface. The resulting disturbance equations obtained by taking the limit as $(\alpha_d\ Re_{ref}) \to \infty$ are called the inviscid equations since they are identical with the equations obtained by ignoring altogether viscosity and thermal conductivity.

Consider a point on the surface of a body on which there develops a three-dimensional boundary layer. It is assumed that the profile of the steady laminar boundary layer is known at this point in terms of the component profiles in two mutually orthogonal surface coordinate directions x and z as shown in Fig. 2. The velocities in the x- and z-directions are u and w, respectively. The resultant external velocity $\sqrt{U_e^2 + W_e^2}$ makes an angle $\psi = \tan^{-1}(W_e/U_e)$ with the x-axis. Now examine the disturbance taken to be an oblique plane wave propagating at an angle θ relative to the x-direction. Any fluctuating quantity F (velocity, temperature, density, etc.) may be described by the complex relation (see Ref. 38 for clarification)

$$F(x,y,z,t) = f(y) \exp\left[i\alpha_d\ (x \cos\theta + z \sin\theta - ct)\right] \tag{1}$$

where f(y) denotes the fluctuation amplitude, α_d the wave number of the disturbance, and c the disturbance propagation velocity. The wave number α_d is considered as a real quantity, while the propagation velocity c is complex. Disturbances are termed to be neutral for $c_i = 0$ where c_i denotes the imaginary part of the propagation velocity c, i.e.,

$$c = c_r + ic_i \tag{2}$$

with c_r denoting the real part (which is physically the phase velocity of wave propagation); disturbances are amplified for $c_i > 0$ and damped for $c_i < 0$. For the condition $c_i < 0$ the corresponding flow is stable for a given value of α_d, whereas $c_i > 0$ denotes instability. The limiting case $c_i = 0$ corresponds to neutral disturbances so that the locus of $c_i = 0$ can be considered as separating the region of stable from that of unstable disturbances.

Restricting attention to the case of a neutral inviscid oscillation at $\alpha_d \, Re_{ref} \to \infty$, Reshotko (Refs. 37 and 38) shows that the necessary and sufficient condition for the existence of a neutral purely inviscid oscillation ($\alpha_d \, Re_{ref} \to \infty$) is

$$A_c \equiv \frac{\overline{W}_c''}{\overline{W}_c'} - \frac{\overline{T}_c'}{\overline{T}_c} = 0 \tag{3}$$

where

$$\overline{W} = \frac{\overline{u} + \overline{w} \tan \theta \tan \psi}{1 + \tan \theta \tan \psi} \tag{4}$$

$$\overline{u} = u/U_e \tag{5}$$

$$\overline{w} = w/W_e \tag{6}$$

$$\overline{T} = T/T_e \tag{7}$$

$$\tan \psi = W_e/U_e \tag{8}$$

with primes denoting differentiation with respect to y, i.e., $\overline{W}' = d\overline{W}/dy$, and subscript c denoting that the required quantities are to be evaluated at the so-called "critical point" where $\overline{W}_c = c_r/[\overline{U}_e \cos(\theta - \psi)]$ which occurs at the so-called "critical height" y_c from the surface. See Fig. 2 for clarification of nomenclature.

Now recall the findings of Stuart in Ref. 36 discussed previously with respect to the formation of a stationary wave caused by the coincidence of the point of inflection of the rotated velocity profile with the y-axis at the critical height location y_c. Application of this concept to the three-dimensional compressible boundary layer for a neutral purely inviscid oscillation ($\alpha_d \, Re_{ref} \to \infty$) forming a stationary wave requires that

$$A_c = \frac{\overline{W}_c''}{\overline{W}_c'} - \frac{\overline{T}_c'}{\overline{T}_c} = 0 \tag{9}$$

and

$$\overline{W}_c = c_r/[U_e \cos(\theta_c - \psi)] = 0 \tag{10}$$

at the critical height location y_c. Equation (4) shows that

$$\tan \theta_c = -\overline{u}_c/[\overline{w}_c \tan \psi] \tag{11}$$

under the restriction of Eq. (10) so that Eq. (9) may be written as

$$A_c = \frac{\dfrac{\overline{u}_c''}{\overline{u}_c} - \dfrac{\overline{w}_c''}{\overline{w}_c}}{\dfrac{\overline{u}_c'}{\overline{u}_c} - \dfrac{\overline{w}_c'}{\overline{w}_c}} - \frac{\overline{T}_c'}{\overline{T}_c} = 0 \tag{12}$$

which becomes the controlling relationship for the location of the critical height y_c. With y_c known, Eq. (11) may be used to determine the stationary wave propagation angle θ_c. For this choice of direction the phase velocity of the neutral disturbance vanishes so as to form a stationary wave.

For the case of incompressible three-dimensional boundary-layer flow at constant temperature, Eq. (12) shows that the condition for the formation of a stationary wave based on a neutral purely inviscid oscillation (α_d $Re_{ref} \rightarrow \infty$) becomes

$$\frac{\bar{u}_c''}{\bar{u}_c} = \frac{\bar{w}_c''}{\bar{w}_c} \tag{13}$$

which is in agreement with the findings of Stuart in Ref. 36 as well as the discussion by Moore (Ref. 39). An experimental study by Gregory and Walker reported in Ref. 36 considered the case of a disk rotating in an incompressible fluid at rest which revealed, by a china-clay technique, the formation of stationary vortices following the shape of logarithmic spirals. Comparison of these experimental results with the neutral inviscid stationary wave analysis by Stuart using essentially Eqs. (11) and (13) above yielded qualitative agreement in that the computed wave propagation angle θ_c agreed with the measured direction within one degree. The analysis of Ref. 36 includes a variational technique for determination of the wavelength of the stationary disturbance. For the rotating disk case, the wavelength computed is four times too short, as compared with the experimental result. The authors of Ref. 36 ascribe this discrepancy to viscosity (which has been neglected in the inviscid-type analysis). However, it is also feasible that the longer wavelength disturbance may simply be more strongly amplified, viscosity being neglected; in plane flow one finds in general that waves of lengths longer than that of the neutral disturbance are amplified at infinite Reynolds number.

2.3 CORRELATION OF DISTANCE TO ONSET OF VORTEX FORMATION IN THE THREE-DIMENSIONAL LAMINAR BOUNDARY LAYER

As stated in Section I, one of the main objectives of the present study concerns the influence of three-dimensional crossflow effects on the formation of streamwise-directed entrained vortices in the laminar boundary layer on a sharp cone at incidence in hypersonic flow. The previous subsection has shown that three-dimensional crossflow has an adverse effect on laminar boundary-layer stability in that a system of streamwise vortices contained within the boundary layer may be formed, apparently because of the inflection point in the rotated velocity profile which is unstable to small disturbances. The exact location at which this vortex system will originate cannot be determined from classical boundary-layer stability theory such as presented in the previous subsection.

Instead, the abrupt formation of these vortices and also the development of complete turbulence, i.e., transition, in a three-dimensional boundary layer can apparently be correlated with a so-called maximum local crossflow Reynolds number, χ_{max}, defined as (Refs. 40 and 41)

$$\chi_{max} = \frac{\rho_e \; w_{s\ell,max} \; \delta}{\mu_e} \tag{14}$$

where $w_{s\ell,max}$ is the maximum crossflow velocity in the streamline coordinates of Fig. 1, and δ is the boundary-layer thickness defined as the normal distance from the surface where the total resultant velocity

$$\sqrt{u^2 + w^2}$$

reaches 0.995 of the total resultant inviscid edge velocity

$$\sqrt{U_e^2 + W_e^2}$$

ρ_e and μ_e are the values of density and viscosity, respectively, evaluated at the inviscid edge conditions. Owen and Randell (Ref. 40) found the critical value of crossflow Reynolds number for vortex formation and for crossflow-induced transition to be 125 and 175, respectively, on swept wings at subsonic speeds. The work by Chapman (Ref. 41) on swept cylinders at supersonic speeds (free-stream Mach numbers up to seven) indicates that

$$\chi_{max} < 100 \Rightarrow \text{Laminar Boundary Layer}$$

$$100 \leqq \chi_{max} \leqq 200 \Rightarrow \text{Vortex Formation and Transitional Boundary Layer}$$

$$\chi_{max} > 200 \Rightarrow \text{Turbulent Boundary Layer}$$

which means that the critical crossflow stability criterion of Owen and Randell may be expected to apply for both subsonic and supersonic flows. Chapman further found that the amount of crossflow needed to induce crossflow instability downstream of the leading edge was very small - on the order of one to five percent of the inviscid edge velocity for the conditions observed. This means physically that on swept wings with large spanwise pressure gradients, as well as sharp and blunt cones at incidence with strong circumferential pressure gradients, boundary-layer transition is more likely to be caused by instability of the crossflow than by instability of the streamwise velocity profile (i.e., Tollmien-Schlichting instability) because of the extremely small amount of crossflow needed to cause transition at small values of the local Reynolds number.

SECTION III
ANALYTICAL ANALYSIS

The present analytical investigation employs a three-dimensional laminar boundary-layer analysis coupled with a three-dimensional inviscid conical flow analysis for a sharp cone at incidence in a hypersonic stream. Each of these analyses utilizes a documented digital computer code which will now be briefly described for sake of completeness.

3.1 INVISCID FLOW

A recent investigation by Jones (Ref. 42) resulted in an accurate and efficient numerical integration procedure for solution of the governing partial differential equations

describing the supersonic or hypersonic inviscid flow field around a sharp cone at incidence. Basically Jones' method uses the condition of conicity to reduce the problem to a set of elliptic nonlinear partial differential equations in two independent variables. A transformation of coordinates is used to fix the boundaries, one of which is the unknown shock wave, between which the elliptic equations are to be satisfied. This transformation also has the effect of including the body shape in the coefficients of the partial differential equations and in the boundary conditions, so that the same method can be used for general conical body shapes simply by changing a few program statements to redefine the equation of the body. In fact, the method is, in many cases, only limited by locally supersonic cross-flow conditions, by the entropy singularity moving too far away from the surface, or by the shock approaching very close to the Mach wave. In practice, these restrictions limit the allowable angle-of-attack range to $\alpha/\delta_v \leqq 1$ (see Fig. 3 for clarification of nomenclature).

At the present time the method has been used successully for circular cones and for bodies that can be obtained by successive perturbations of a circular cone and that do not have curvatures that are too large. Jones (Ref. 42) has reported examples for circular cones at incidence, elliptic cones, and a body whose cross-sectional shape is represented by a fourth-order even-cosine Fourier series.

The method is efficient in computer time compared with other fully numerical techniques, and one solution takes from one-half minute to three minutes on an IBM 360/50 computer for the circular cone at incidence - the time increasing as the incidence increases. This is to be compared with a time requirement of approximately one-half hour on an IBM 360/50 computer for the technique developed by Moretti (Ref. 43) in which the flow-field solution is obtained by marching step by step downstream (approximately 400 downstream steps are required) until a conicity condition is sufficiently well satisfied. Comparison of results between the Jones and Moretti approaches shows excellent agreement, with the Jones digital computer code being a factor of approximately ten faster than the Moretti approach in solution time. An analysis very similar to that of Jones has recently been reported by South and Klunker (Ref. 44) while Holt and Ndefo (Ref. 45) have developed a method of integral relations approach to the problem. The important point to note is that all of the above-referenced analyses report excellent agreement with experiment for sharp circular and elliptic cones at incidence under supersonic and hypersonic flow conditions so that the choice of which analysis is indeed the best remains an open question. The present author's experience with use of the Jones digital computer code (Ref. 46) has been most favorable from a user's standpoint.

It should be pointed out in conclusion that Jones (Ref. 47) has recently published a very complete and thorough set of tables for inviscid supersonic and hypersonic flow about circular cones at incidence in a perfect gas, $\gamma = 1.40$, stream.

3.2 VISCOUS BOUNDARY-LAYER FLOW

As discussed in Section I, digital computer codes are now available (see Refs. 11 through 25) for accurate numerical solution of the three-dimensional laminar boundary-layer equations. For application in the present sharp cone investigation, the

three-dimensional conical flow laminar boundary-layer analysis presented in Appendix B of McGowan and Davis (Ref. 25) has been used. This treatment is very similar to that of Dwyer (Ref. 17) and Boericke (Ref. 23) in that the limiting conical form of the full three-dimensional compressible laminar boundary-layer equations as originally derived by Moore (Ref. 9) is solved using an implicit finite-difference technique for numerical integration of the nonlinear parabolic partial differential equations written in similarity variable form. This similarity variable transformation reduces the number of independent variables from three to two in the transformed governing equations so that the problem becomes two-dimensional in form. Since there are only two independent variables in this coordinate system, the implicit finite-difference techniques developed by Blottner (Refs. 48 and 49) can be used almost directly to solve the governing equations. The complete formalism of this numerical approach is discussed in Chapter III of the report by McGowan and Davis (Ref. 25) to which the reader is referred for further study.

The necessary outer-edge conditions for input to the above boundary-layer analysis are determined based on results from the Jones inviscid sharp cone at incidence analysis discussed in Section 3.1. The procedure for specifying the inviscid data necessary for input to the McGowan and Davis boundary-layer analysis is quite simple in that only the pressure distribution around the cone, along with the velocity and density on the windward streamline, must be specified. All other inviscid quantities are then internally calculated using the inviscid compressible Bernoulli and crossflow momentum equations applied at the surface along with the restriction that the entropy remain constant on the surface; i.e., the cone surface is an isentropic surface. Complete details of this procedure are given in Section B of Chapter IV in the report by McGowan and Davis (Ref. 25).

The gas is assumed to be both thermally and calorically perfect air having a constant ratio of specific heats $\gamma = 1.40$. The gas viscosity is assumed to obey the Sutherland viscosity law for air, while the Prandtl number of the gas is taken to be constant at a value of 0.71. The wall temperature of the cone is assumed to remain constant around the cone at a value prescribed by input to the analysis.

Experience with the McGowan and Davis digital computer code reported in Ref. 25 has revealed few defects, and the present author highly recommends its use. It should be noted that the main emphasis of Ref. 25 is placed upon development and documentation of a very general three-dimensional laminar boundary-layer analysis for general body geometry, providing the inviscid flow field for the body in question is available from some source.

SECTION IV
BODY AND FLOW CONDITIONS

Most of the experimental data reported by McDevitt and Mellenthin in Ref. 5 was taken in the NASA Ames 3.5-foot Hypersonic (Air) Tunnel on both ablating and nonablating sharp cone models under hypersonic conditions. For the present investigation and comparison of theory with the experimental data of Ref. 5, only nonablating sharp cones with semivertex angles of 5, 10, and 15 deg will be considered; all of the sharp cones have base diameters of 3.0 in. Only angles of attack less than or equal to the sharp

cone semivertex angle can be analyzed using the Jones inviscid sharp cone at incidence analysis (Ref. 42) discussed in Section 3.1, so that the current investigation is restricted to the angle-of-attack range $\alpha/\delta_v \leqq 1$; see Figs. 3 and 4 for the sharp cone geometry and general nomenclature.

All of the experimental data for air presented in Ref. 5 were taken at a nominal free-stream Mach number, M_∞, of 7.4 and free-stream Reynolds numbers based on model length, $Re_{\infty,L}$, of 0.5×10^6 and 3.0×10^6. The nominal wall-to-stagnation-temperature ratio, T_w/T_o, was 0.3, which represents a relatively cold wall condition. All of the present calculations have been performed for these nominal flow conditions except for the high Reynolds number ($Re_{\infty,L} = 3.0 \times 10^6$) condition which used an exact $T_w/T_o = 0.2857$ instead of the nominal 0.30 value.

SECTION V
RESULTS AND DISCUSSION

Typical comparisons of analytical results from the Jones (Refs. 42 and 46) and McGowan and Davis (Ref. 25) analyses relative to the experimental data of McDevitt and Mellenthin (Ref. 5) for sharp cones at incidence in a hypersonic flow will now be presented. The flow conditions used in the calculations are those presented in Section IV and correspond to the experimental conditions.

The surface upwash angles for 5-, 10-, and 15-deg half-angle sharp cones at various incidence angles are given in Figs. 5 and 6; definition of the upwash angle may be found in Figs. 3 and 4 where ϵ_i denotes the inviscid upwash angle based on the Jones inviscid sharp cone at incidence analysis (Refs. 42 and 46) and ϵ_s denotes the surface upwash angle which corresponds to the measured oil-flow results as well as the calculated values from the McGowan and Davis (Ref. 25) laminar boundary-layer analysis. Comparison of Figs. 5 and 6 reveals that for these flow conditions the maximum surface upwash angle is approximately a factor of four greater than the calculated maximum inviscid upwash angle. This is a clear indication of the large amounts of crossflow present in these three-dimensional laminar boundary layers. Further note that the angular location ϕ of maximum upwash angle increases as the angle of incidence increases due to increasing three-dimensional crossflow. In general, the agreement between the calculated and measured surface upwash angles in Fig. 6 is excellent over the windward (0 deg $\leqq \phi \leqq$ 90 deg) half of all three cones. As the angle of incidence is increased for a given cone, progressive disagreement between calculated and measured values at the ϕ = 135 deg location is observed, especially for the δ_v = 5 deg case. It is suspected that the crossflow instability phenomenon discussed in Section II may be causing premature boundary-layer transition in the manner presented later in the present section. The free-stream Reynolds number is sufficiently low for these cases ($Re_{\infty,L} = 5 \times 10^5$) that one would certainly expect a priori a laminar boundary layer over the entire cone. One way to accurately assess if indeed crossflow-induced transitional flow is present at, say, the ϕ = 135 deg angular location for the 5-deg half-angle sharp cone at 4-deg angle of attack, is to experimentally measure the circumferential heat-transfer distribution around the cone for comparison with the McGowan and Davis three-dimensional laminar boundary-layer analysis (Ref. 25).

The above-discussed results reveal quite clearly the applicability and accuracy of the present analysis technique for three-dimensional laminar boundary layers on sharp cones under cold wall conditions. As McDevitt and Mellenthin point out in Ref. 5, the effect of changes in flow enthalpy at the wall on surface upwash angles may be quite significant, i.e., the surface upwash angle may be changed by as much as 50 percent between hot and cold wall conditions. Shown in Fig. 7 are the calculated upwash angle distributions around a 10-deg half-angle sharp cone at 5-deg angle of attack for various values of the wall temperature ratio. Also presented in Fig. 7 is the corresponding inviscid surface upwash angle for sake of comparison. Note that the upwash angle for the "hot" $T_w/T_o = 0.90$ condition is approximately three times the value for the "cold" $T_w/T_o = 0.0$ case. Further note that the angular location of maximum upwash angle shifts from $\phi \approx 110$ deg for the "cold" $T_w/T_o = 0.0$ condition to $\phi \approx 120$ deg for the "hot" $T_w/T_o = 0.90$ case. A cross-plot of the data in Fig. 7 is shown by Fig. 8 in terms of the surface upwash angle variation with wall temperature ratio for a given angular location. The important point to note from these two figures is that the three-dimensional laminar boundary layer on a sharp cone at incidence is extremely sensitive to the wall temperature level with respect to the amount of turning due to crossflow. This has important implications in connection with hypersonic wind tunnel testing under hot wall conditions relative to flight cold wall conditions for such aerodynamic parameters as static-stability coefficients on lifting reentry configurations at incidence, as will be discussed at greater length later in this section.

As discussed in Section I, McDevitt and Mellenthin (Ref. 5) experimentally observed via an oil-film technique the formation of entrained vortices in the three-dimensional laminar boundary layer on sharp cones at incidence under cold wall, high Reynolds number, hypersonic wind tunnel conditions. The measured upward inclination of these vortices was considerably less than the corresponding inclination of the surface streamlines but somewhat greater than the calculated inviscid upwash angle at the outer edge of the boundary layer. As presented in Section 2.2, three-dimensional compressible boundary-layer stability theory following Refs. 37 and 38 can be applied through Eqs. (11 and 12) to determine neutral purely inviscid oscillations forming a stationary wave which the results of Ref. 36 show to be in qualitative agreement with the measured direction of stationary vortices formed on a rotating disk in an incompressible fluid at rest.

At this point the stability theory of Section 2.2 will be applied to the sharp cone flows of Ref. 5 with respect to angular orientation of the stationary vortices formed due to crossflow instability. The controlling relationship for the location of the critical height y_c at which the phase velocity of the neutral disturbance vanishes so as to form a stationary wave entrained within the three-dimensional boundary layer is given by Eq. (12) solely in terms of the boundary-layer axial and circumferential velocity profiles and their derivatives as well as the boundary-layer static temperature profile and its derivative. Presented in Tables I through IV are the tabulated boundary-layer profiles based on the three-dimensional laminar boundary-layer analysis of McGowan and Davis (Ref. 25) applied to the four cases for which McDevitt and Mellenthin (Ref. 5) present experimental results for vortex angular orientation, namely the $\phi = 90$-deg body location on a 10-deg half-angle sharp cone at 5-deg, 6-deg, and 8-deg angles of attack as well as a 15-deg half-angle sharp cone at 5-deg angle of attack. It is to be noted that the velocity profiles in Tables I

through IV are relative to the body fixed coordinate system of Figs. 3 and 4. Use of these profiles in Eq. (12) to determine the critical height y_c which is then used in Eq. (11) to determine the stationary wave propagation angle θ_c yields the calculated vortex angles ϵ_v (where ϵ_v = 90 deg + θ_c) shown in Fig. 9 denoted as x symbols; see Figs. 3 and 4 for clarification of the vortex angle ϵ_v definition. For the 10-deg half-angle sharp cone, the three-dimensional inviscid neutral stationary disturbance theory lies some 15 to 18 percent (one to two degrees) below the measured vortex angular orientation at the ϕ = 90-deg location. However, the trend of increasing vortex angle with increasing angle of attack is reasonably well predicted by the theory. For the 15-deg half-angle sharp cone, a 45-percent discrepancy (four degrees) between the three-dimensional inviscid neutral stationary disturbance theory and experiment is observed at the ϕ = 90-deg location.

The exact reason behind the above-indicated discrepancy between theory and experiment with respect to the angular orientation of the vortex path is not clear. Several possibilities exist relative to application of Reshotko's three-dimensional compressible boundary-layer stability theory under hypersonic conditions. For free-stream Mach numbers above two or three, it has been pointed out by several investigators (Refs. 34, 35, 50, 51, and 52) that the compressible stability equations include a number of terms, involving the component of the mean boundary-layer velocity perpendicular to the surface, which are not negligible, but have been ignored in making parallel flow assumptions such as used by Reshotko (Refs. 37 and 38). The effort of this vertical velocity component can become very important under high Mach number conditions as shown by Brown (Ref. 52). In addition, the present application of Reshotko's analysis is valid only in the neutral inviscid stationary disturbance sense which requires that $\alpha_d \, Re_{ref} \rightarrow \infty$ (see Section 2.2). At present it is not known under what circumstances and with what accuracy the inviscid theory can be applied at finite Reynolds number under hypersonic conditions. It would be of great interest to apply the analysis by Brown (Ref. 52) to the present problem of stationary vortex formation since Brown includes all terms in a complete set of three-dimensional stability equations allowing viscous effects (such as dissipation which becomes of increasing importance under cold wall hypersonic conditions). In this connection the tabulated three-dimensional laminar boundary-layer profiles given in Tables I through IV (Appendix II) of the present report are necessary input to such an analysis.

In order to gain some physical insight into the calculated results from application of three-dimensional neutral inviscid stability theory for stationary disturbances, Fig. 10 shows the location of the critical height y_c relative to the degree of turning due to crossflow in the three-dimensional laminar boundary layer at the circumferential location ϕ = 90 deg on a 10-deg half-angle sharp cone at 6-deg angle of attack. Note that the critical height is located near the outer edge of the boundary layer, i.e., $y_c/\delta \approx 0.80$, which means physically that the stationary disturbance (vortex) formation is probably not a viscous-dominated phenomenon and hence may be adequately described by an appropriate inviscid theory. It is interesting to observe that the critical height location in Fig. 10 for a three-dimensional stationary disturbance is in reasonable agreement with the experimentally determined critical heights presented by Potter and Whitfield (Ref. 53) for nonstationary disturbance formation in two-dimensional hypersonic laminar boundary layers. Since this agreement between two- and three-dimensional flows is probably fortuitous, it would be of great value to conduct an experimental hot-wire probe

investigation similar to that reported by Potter and Whitfield for the present case of three-dimensional stationary disturbances in order to experimentally determine the critical height y_c for comparison with three-dimensional neutral inviscid stability theory.

As discussed in Section 2.2 the exact location at which the stationary vortex system will originate cannot be determined from classical boundary-layer stability theory so that recourse must be taken to application of the maximum local crossflow Reynolds number χ_{max} in order to correlate the onset of vortex formation. Recall from Section 2.3 that

$$\chi_{max} < 100 \Rightarrow \text{Laminar Boundary Layer}$$

$$100 \leqq \chi_{max} \leqq 200 \Rightarrow \text{Vortex Formation and Transitional Boundary Layer}$$

$$\chi_{max} > 200 \Rightarrow \text{Turbulent Boundary Layer}$$

based on the criterion by Chapman (Ref. 41). Presented in Fig. 11 are the calculated maximum local crossflow Reynolds number distributions around two sharp cones at incidence (δ_v = 10 deg at α = 5 deg and δ_v = 15 deg at α = 5 deg) for which McDevitt and Mellenthin (Ref. 5) present photographic documentation of the onset to vortex formation based on an oil-film technique. Note that Fig. 11 is given in laminar boundary-layer similarity format; i.e., χ_{max} is divided by $\sqrt{x/L}$. From Fig. 11 and the criterion by Chapman reiterated above, a developed surface plot with lines of constant χ_{max} can easily be formulated with respect to location of onset to vortex formation. Such is presented in Fig. 12 for the two sharp cones at incidence of present interest. Lines of constant χ_{max} = 100 and 200 are shown up to the ϕ = 90-deg circumferential location in order to delineate the region of expected onset to vortex formation. It is extremely difficult to accurately read the McDevitt and Mellenthin photographs with respect to actual initial onset of a vortex streak. Only two such points are presented for the 10-deg sharp cone case. However, for the 15-deg sharp cone sufficient data are available to form the shaded band shown in Fig. 12. Based on these results it appears that vortex formation may be expected on sharp cones at incidence under conditions where χ_{max} assumes values greater than approxiamtely 150. It is impossible to ascertain if the boundary layer becomes turbulent for $\chi_{max} > 200$ based on the McDevitt and Mellenthin data. What is needed here for completeness are heat-transfer measurements in the region of vortex formation and downstream in order to clearly delineate the state of the boundary layer.

It is extremely important to note from Fig. 12 that the maximum crossflow Reynolds number concept coupled with the three-dimensional laminar boundary-layer analysis correctly predicts the trend observed in the experimental data of Refs. 3 and 4 that the transition movement undergoes a much more rapid forward progression on the leeward side than the rearward progression for the windward side of sharp cones at incidence in hypersonic flow; see the sketch in Section I for clarification. The only other work, to the present author's knowledge, along the same lines as the above application of the maximum crossflow Reynolds number concept to prediction of stability boundaries for aerodynamic bodies of revolution at incidence is a paper by Nachtsheim (Ref. 54) for

incompressible flow over a paraboloid of revolution at small-angles of attack based on the small crossflow approximation.

Another important facet of the crossflow instability phenomenon is the influence of wall temperature level on the magnitude of the calculated maximum crossflow Reynolds number χ_{max}. As shown very clearly in Fig. 13, increasing wall temperature level at a given circumferential location increases the value of χ_{max} and hence makes the three-dimensional laminar boundary layer more susceptible to crossflow instability leading to vortex formation and transition. The reason behind this behavior can be seen from Figs. 14 and 15 which present the variation of the maximum crossflow velocity (in streamline coordinates) and the boundary-layer thickness (in similarity form) with respect to wall temperature for three different circumferential locations around the cone. Note that the maximum crossflow velocity is increased by approximately a factor of three while the boundary-layer thickness is increased by approximately a factor of two as the wall temperature level is increased from $T_w/T_o = 0.0$ to $T_w/T_o = 0.90$. Since, from Eq. (14),

$$\chi_{max} = \frac{\rho_e \; w_{s\ell,max} \; \delta}{\mu_e}$$

with ρ_e and μ_e being determined by the local inviscid edge conditions (which, of course, are independent of wall temperature level), the above results reveal that the increase of the maximum crossflow Reynolds number with wall temperature level at a given circumferential location as shown in Fig. 13 is totally due to the sensitivity of the three-dimensional laminar boundary-layer crossflow velocity profile and boundary-layer thickness to changes in the wall temperature level. In general, the hotter the wall, the greater the crossflow velocity and boundary-layer thickness which leads to greater instability (due to increasing crossflow effects) in the three-dimensional laminar boundary layer.

It is very important to recognize from Fig. 13 that severe wall cooling ($T_w/T_o \rightarrow 0$) can render the present sharp cone ($\delta_v = 10$ deg at $\alpha = 5$ deg) stable to three-dimensional crossflow instability over the entire body for the given flow conditions based on a value of $\chi_{max} > 150$ required for onset to vortex formation. Recalling the significant influence of boundary-layer transition on slender bodies at incidence relative to static-stability characteristics as discussed in Refs. 2, 3, and 4, the results of Fig. 13 give warning that static-stability ground testing in hypersonic wind tunnels under hot wall conditions on slender bodies at incidence may not be applicable to cold wall flight conditions due to the crossflow instability phenomenon. Much more work remains to be done in this area before a definite conclusion on this potential problem area in relating ground test results to actual flight conditions can be reached.

SECTION VI
CONCLUDING SUMMARY

The present investigation was devoted to analysis of experimental measurements concerning surface upwash angles and entrained vortex formation in the three-dimensional

laminar boundary layer on sharp cones at incidence in a hypersonic flow. Excellent agreement with respect to surface upwash angles between three-dimensional laminar boundary-layer theory (applied through numerical integration of the governing three-dimensional equations using an implicit finite-difference technique) and experimental measurements taken in a hypersonic wind tunnel was obtained for angles of attack less than the cone half-angle. The angle-of-attack restriction was due to the three-dimensional inviscid analysis used in the present study to obtain the outer edge conditions for input to the boundary-layer calculations. A strong influence of wall temperature level on the surface upwash angle was found to exist for sharp cones at incidence. In general, the hotter the wall, the greater the turning effect on the three-dimensional laminar boundary layer due to crossflow. This finding has application in the interpretation of results from wind tunnel tests on slender bodies at incidence under hot wall conditions relative to actual flight conditions in a cold wall environment.

Attention was also directed in the present investigation toward application of three-dimensional neutral inviscid stability theory for stationary disturbances in order to calculate the angular orientation of entrained vortices formed in the three-dimensional laminar boundary layer because of crossflow-induced inflectional instability in the rotated boundary-layer velocity profile. Application of this approach was not entirely satisfactory relative to experiment, but more work must be done before declaring the approach invalid; terms which may have been significant under hypersonic conditions were not included in the present stability analysis. The location of the so-called critical height was found to be near the edge of the three-dimensional laminar boundary layer which is a hopeful sign that inviscid stability theory can indeed be applied under hypersonic cold wall conditions.

A so-called maximum crossflow Reynolds number concept was applied in the present analysis to successfully correlate the onset to vortex formation in the three-dimensional laminar boundary layer on sharp cones at incidence. The numerical value of the maximum crossflow Reynolds number at which vortex formation is observed to begin relative to experimental data on sharp cones was found to agree quite well with previous experiments on swept wings and cylinders under subsonic and supersonic conditions. It appears that a value of approximately 175 for the maximum crossflow Reynolds number is sufficient for onset to vortex formation in the three-dimensional laminar boundary layer on sharp cones in hypersonic flow under cold wall conditions.

The actual numerical magnitude of the maximum crossflow Reynolds number was found to be quite sensitive to the wall temperature level with, in general, the hotter the wall, the larger the value for the maximum crossflow Reynolds number and hence the more unstable the three-dimensional laminar boundary layer to the crossflow instability phenomenon. This behavior was shown to be the result of increased boundary-layer crossflow velocity and thickness as the wall temperature is increased. Based on these findings, static-stability ground testing in hypersonic wind tunnels under hot wall conditions on slender bodies at incidence may not be applicable to cold wall flight conditions at the same free-stream Mach and Reynolds number conditions because of the crossflow instability phenomenon being enhanced by the hot wall condition which, in turn, can result in premature transition of the three-dimensional laminar boundary layer to turbulent

flow. What is needed in order to more fully understand this crossflow-induced instability phenomenon and its effects on boundary-layer transition under various wall temperature conditions is a careful and thorough experimental investigation of the three-dimensional laminar boundary-layer structure (profile measurements) as well as surface heat-transfer measurements under flow conditions leading to entrained vortex formation and transition on sharp cones at incidence.

REFERENCES

1. Sherman, M. M. and Nakamura, T. "Flight Test Measurements of Boundary-Layer Transition on a Nonablating 22° Cone." J. Spacecraft and Rockets, Vol. 7, No. 2, February 1970, pp. 137-142.

2. Ericsson, L. E. "Effect of Boundary-Layer Transition on Vehicle Dynamics." J. Spacecraft and Rockets, Vol. 6, No. 12, December 1969, pp. 1404-1409.

3. DiCristina, V. "Three-Dimensional Laminar Boundary-Layer Transition on a Sharp 8° Cone at Mach 10." AIAA J., Vol. 8, No. 5, May 1970, pp. 852-856.

4. Martellucci, A. and Neff, R. S. "The Influence of Asymmetric Transition on Re-Entry Vehicle Motion." AIAA Paper No. 70-987 presented at the AIAA Guidance, Control, and Flight Mechanics Conference, Santa Barbara, California, August 1970.

5. McDevitt, J. B. and Mellenthin, J. A. "Upwash Patterns on Ablating and Nonablating Cones at Hypersonic Speeds." NASA TN D-5346, July 1969.

6. Persen, L. N. "A Simplified Approach to the Influence of Görtler-Type Vortices on the Heat Transfer from a Wall." ARL Report 65-88, May 1965.

7. Persen, L. N. "Streamwise Directed Vortices and Crosshatched Surfaces of Re-Entry Vehicles." J. Spacecraft and Rockets, Vol. 7, No. 1, January 1970, pp. 108-110.

8. Cleary, J. W. "An Experimental and Theoretical Investigation of the Pressure Distribution and Flow Fields of Blunted Cones at Hypersonic Mach Numbers." NASA TN D-2969, August 1965.

9. Moore, F. K. "Three-Dimensional Compressible Laminar Boundary Layer Flow." NACA TN 2279, March 1951.

10. Hayes, W. D. "The Three-Dimensional Boundary Layer." NAVORD Report 1313, May 1951.

11. Der, J., Jr. and Raetz, G. S. "Solution of General Three-Dimensional Laminar Boundary-Layer Problems by an Exact Numerical Method." IAS Paper No. 62-70 presented at the IAS 30th Annual Meeting, New York, January 22-24, 1962.

12. Cooke, J. C. "Supersonic Laminar Boundary Layers on Cones." RAE TR-66347, November 1966.

13. Hall, M. G. "A Numerical Method for Calculating Steady Three-Dimensional Laminar Boundary Layers." RAE TR-67145, June 1967.

14. Powers, S. A., Niemann, A. F., Jr. and Der, J., Jr. "A Numerical Procedure for Determining the Combined Viscid-Inviscid Flow Fields over Generalized Three-Dimensional Bodies." AFFDL-TR-67-124, December 1967.

15. Der, J., Jr. "A Study of General Three-Dimensional Boundary Layer Problems by an Exact Numerical Method." AIAA Paper No. 69-138 presented at the AIAA 7th Aerospace Sciences Meeting, New York, January 20-22, 1969.

16. Dwyer, H. A. "Solution of a Three-Dimensional Boundary-Layer Flow with Separation." AIAA J., Vol. 6, No. 7, July 1968, pp. 1336-1342. See also GE TIS R67SD54, August 1967.

17. Dwyer, H. A. "Boundary Layer on a Hypersonic Sharp Cone at Small Angle of Attack." AIAA J., Vol. 9, No. 2, February 1971, pp. 277-284. See also SC-CR-69-3284, 1969.

18. Dwyer, H. A. and McCroskey, W. J. "Crossflow and Unsteady Boundary-Layer Effects on Rotating Blades." AIAA Paper No. 70-50 presented at the AIAA 8th Aerospace Sciences Meeting, New York, January 19-21, 1970.

19. Krause, E. "Comment on 'Solution of a Three-Dimensional Boundary-Layer Flow with Separation'." AIAA J., Vol. 7, No. 3, March 1969, pp. 575-576.

20. Krause, E., Hirschel, E. H., and Bothmann, Th. "Numerische Stabilität dreidimensionaler Grenzschichtlösungen." ZAMM Sonderheft 48, 1968, pp. T205-T208.

21. Krause, E., Hirschel, E. H., and Bothmann, Th. "Normal Injection in a Three-Dimensional Laminar Boundary Layer." AIAA J., Vol. 7, No. 2, February 1969, pp. 367-369.

22. Krause, E., Hirschel, E. H., and Bothmann, Th. "Differenzenformeln zur Berechnung dreidimensionaler Grenzschichten." DLR FB 69-66, September 1969.

23. Boericke, R. R. "Laminar Boundary Layer on a Cone at Incidence in Supersonic Flow." AIAA J., Vol. 9, No. 3, March 1971, pp. 462-468.

24. Vvedenskaia, N. D. "Calculation of the Boundary Layer Arising in Flow Past a Cone at an Angle of Attack." Zh. Vychisl. Mat. mat. Fiz., Vol. 6, No. 2, 1966, pp. 304-312.

25. McGowan, J. J., III, and Davis, R. T. "Development of a Numerical Method to Solve the Three-Dimensional Compressible Laminar Boundary-Layer Equations with Application to Elliptical Cones at Angle of Attack." ARL Report 70-0341, December 1970.

26. Wilkins, M. E. "Evidence of Surface Waves and Spreading of Turbulence on Ablating Models." AIAA J., Vol. 3, No. 10, October 1965, pp. 1963-1965.

27. Wilkins, M. E. and Tauber, M. E. "Boundary Layer Transition on Ablating Cones at Speeds up to 7 km/sec." AIAA J., Vol. 4, No. 8, August 1966, pp. 1344-1348.

28. Larson, H. K. and Mateer, G. G. "Cross-Hatching - A Coupling of Gas Dynamics with the Ablation Process." AIAA Paper No. 68-670 presented at the AIAA Fluid and Plasma Dynamics Conference, Los Angeles, California, June 24-26, 1968.

29. Canning, T. N., Tauber, M. E., Wilkins, M. E., and Chapman, G. T. "Orderly Three-Dimensional Processes in Turbulent Boundary Layers on Ablating Bodies." AGARD Conference Proceedings No. 30, Hypersonic Boundary Layers and Flow Fields, May 1968, pp. 6-1 through 6-14.

30. Laganelli, A. L. and Nestler, D. E. "Surface Ablation Patterns: A Phenomenology Study." AIAA J., Vol. 7, No. 7, July 1969, pp. 1319-1325.

31. Tobak, M. "Hypothesis for the Origin of Cross-Hatching." AIAA J., Vol. 8, No. 2, February 1970, pp. 330-334.

32. Persen, L. N. "Investigation of Streamwise Vortex Systems Generated in Certain Classes of Curved Flow, Part 1." ARL 68-0134, July 1968.

33. Jaffe, N. A., Okamura, T. T., and Smith, A. M. O. "Determination of Spatial Amplification Factors and Their Application to Predicting Transition." AIAA J., Vol. 8, No. 2, February 1970, pp. 301-308.

34. Mack, L. M. "Boundary-Layer Stability Theory." JPL/CIT 900-277 Rev. A, November 1969.

35. Morkovin, M. V. "Critical Evaluation of Transition from Laminar to Turbulent Shear Layers with Emphasis on Hypersonically Traveling Bodies." AFFDL-TR-68-149, March 1969.

36. Gregory, N., Stuart, J. T., and Walker, N. S. "On the Stability of Three-Dimensional Boundary Layers with Application to the Flow Due to a Rotating Disk." Phil. Trans. Royal Society (London), Series A, Vol. 248, No. 943, July 1955, pp. 155-199.

37. Reshotko, E. "Stability of Three-Dimensional Compressible Boundary Layers." NASA TN D-1220, June 1962.

38. Reshotko, E. "Stability of the Compressible Laminar Boundary Layer." GALCIT Hypersonic Research Project Memorandum No. 52, January 1960.

39. Moore, F. K. "Three-Dimensional Boundary Layer Theory." Advances in Applied Mechanics, Vol. IV, Academic Press, Inc., New York, 1956, pp. 159-228.

40. Owen, P. R. and Randall, D. G. "Boundary Layer Transition on a Swept-Back Wing." RAE TM Aero. 277, May 1952.

41. Chapman, G. T. "Some Effects of Leading-Edge Sweep on Boundary Layer Transition at Supersonic Speeds." NASA TN D-1075, September 1961.

42. Jones, D. J. "Numerical Solutions of the Flow Field for Conical Bodies in a Supersonic Stream." National Research Council of Canada Aeronautical Report LR-507, July 1968. See also C.A.S.I. Transactions, Vol. 3, No. 1, March 1970, pp. 62-71.

43. Moretti, G. "Inviscid Flow Field Past a Pointed Cone at Angle of Attack. Part I-Analysis." GASL TR-577, December 1965. See also AIAA J., Vol. 5, No. 4, April 1967, pp. 789-791.

44. South, J. C., Jr. and Klunker, E. B. "Methods for Calculating Nonlinear Conical Flows." Paper 8 in "Analytic Methods in Aircraft Aerodynamics." NASA SP-228, Symposium held at NASA Ames Research Center, Moffett Field, California, October 28-30, 1969, pp. 131-158.

45. Holt, M. and Ndefo, D. E. "A Numerical Method for Calculating Steady Unsymmetrical Supersonic Flow Past Cones." J. Computational Physics, Vol. 5, 1970, pp. 463-486.

46. Jones, D. J. "Use of the Jones Computer Programme to Determine the Flow Field for Conical Flow Situations. Part I: The Circular Cone at Incidence." National Research Council of Canada NAE LTR-HA-1, June 1969.

47. Jones, D. J. "Tables of Inviscid Supersonic Flow About Circular Cones at Incidence $\gamma = 1.4$, Parts I and II." AGARDograph 137, November 1969.

48. Blottner, F. G. "Viscous Shock Layer at the Stagnation Point with Nonequilibrium Air Chemistry." AIAA J., Vol. 7, No. 12, December 1969, pp. 2281-2288.

49. Blottner, F. G. "Finite Difference Methods of Solution of the Boundary-Layer Equations." AIAA J., Vol. 8, No. 2, February 1970, pp. 193-205.

50. Cheng, S.-I. "On the Stability of Laminar Boundary Layer Flow." Quart. Appl. Math., Vol. 11, No. 3, October 1953, pp. 346-350.

51. Dunn, D. W. and Lin, C. C. "On the Stability of the Laminar Boundary Layer in a Compressible Fluid." J. Aero. Sci., Vol. 22, No. 7, July 1955, pp. 455-477.

52. Brown, W. B. "Stability of Compressible Boundary Layers." AIAA J., Vol. 5, No. 10, October 1967, pp. 1753-1759.

53. Potter, J. L. and Whitfield, J. D. "Effects of Slight Nose Bluntness and Roughness on Boundary-Layer Transition in Supersonic Flow." J. Fluid Mech., Vol. 12, Part 4, April 1962, pp. 501-535.

54. Nachtsheim, P. R. "The Three-Dimensional Boundary Layer on a Body of Revolution at Small Incidence and Its Stability." Developments in Mechanics, Vol. 2, Part 1, Fluid Mechanics, Proceedings of the Eighth Midwestern Mechanics Conference held at Case Institute of Technology, April 1-3, 1963, Pergamon Press, Inc., New York, 1965, pp. 306-339.

APPENDIXES

I. ILLUSTRATIONS

II. TABLES

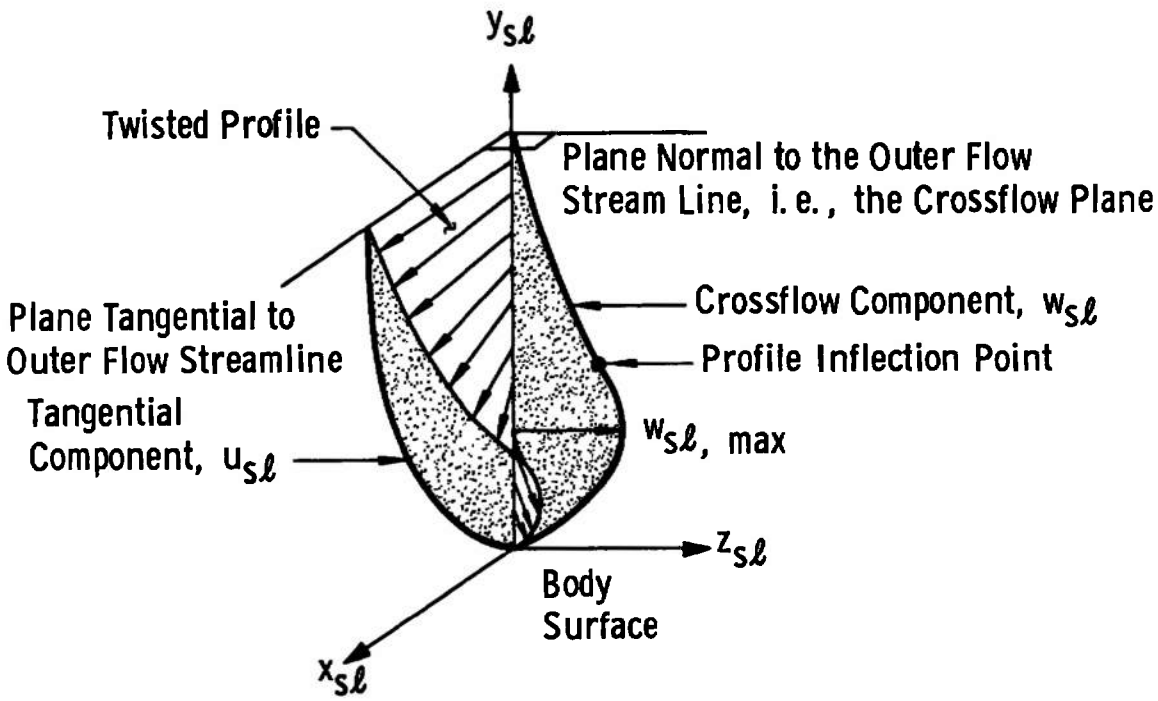

Fig. 1 Three-Dimensional Boundary-Layer Velocity Profiles in Streamline Coordinates

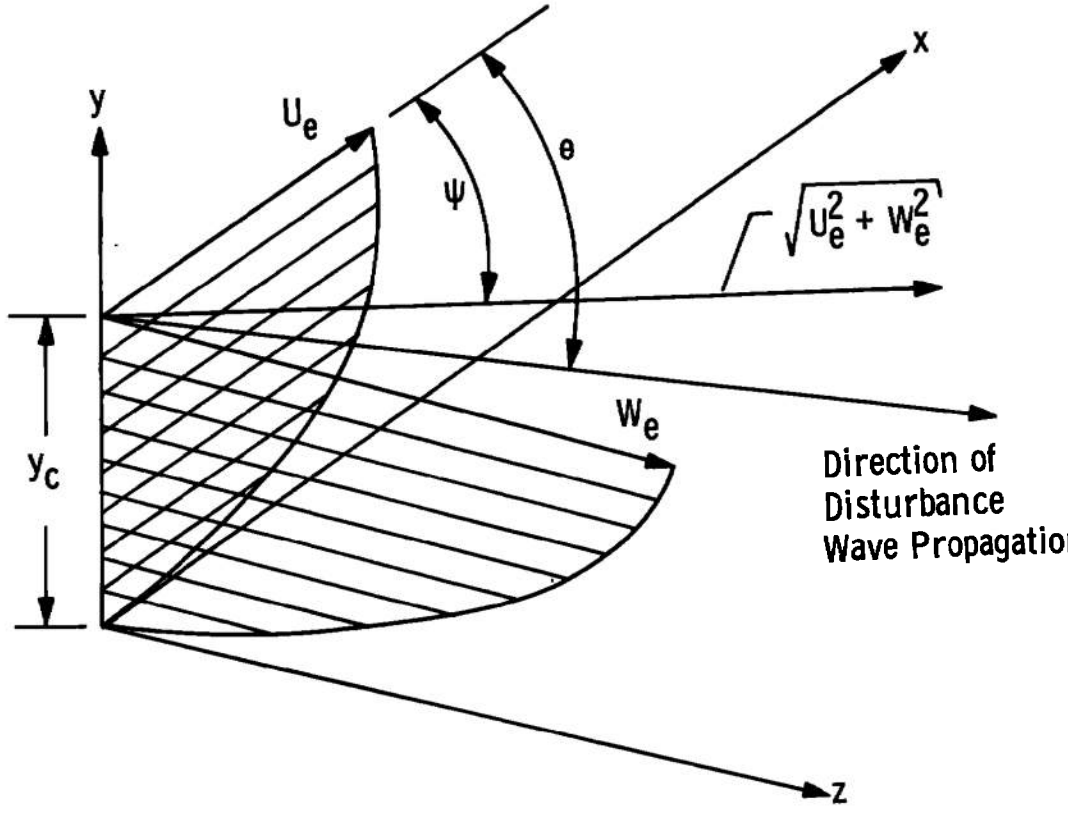

Fig. 2 Schematic of Disturbance Wave Propagation in a Three-Dimensional Boundary Layer

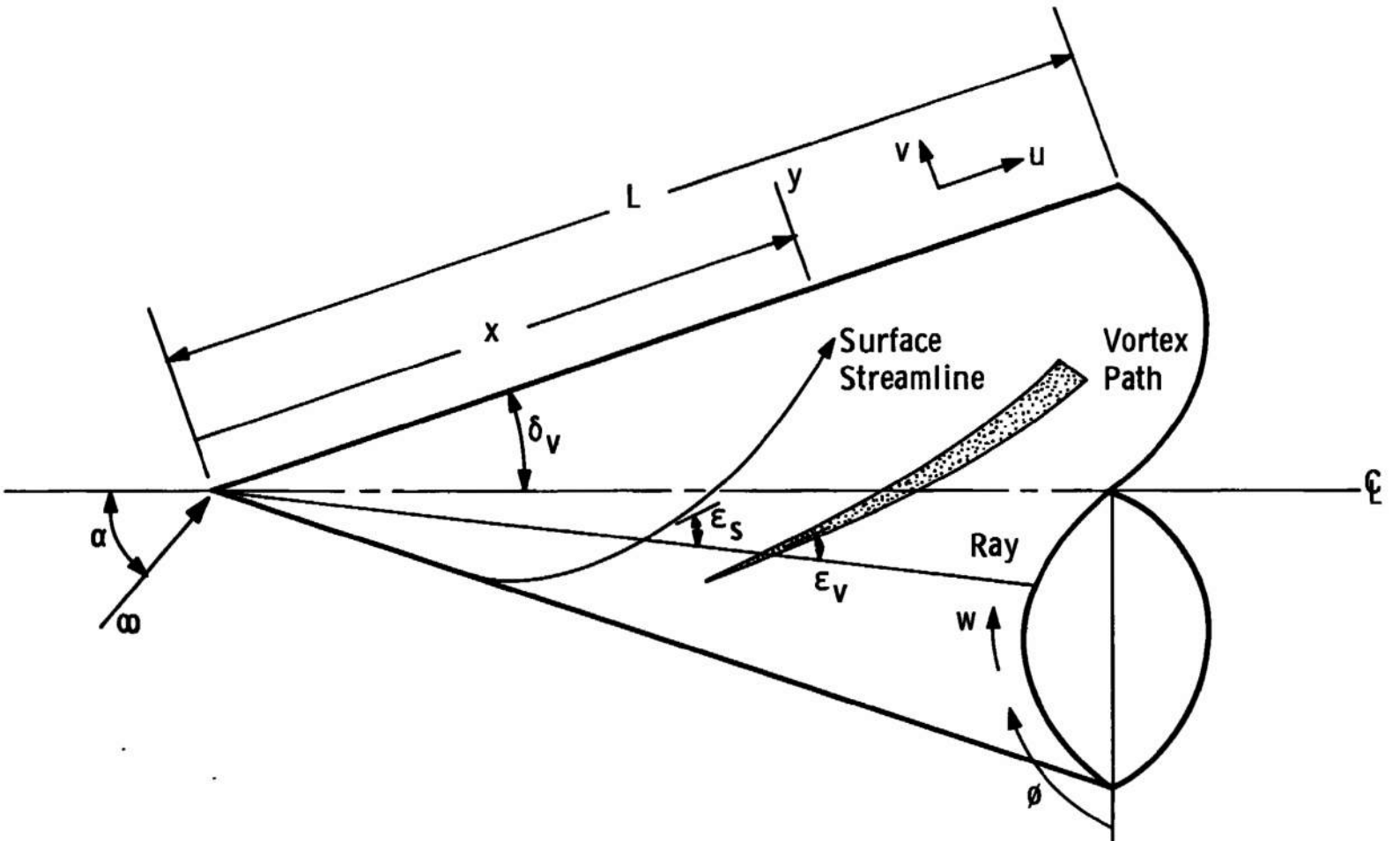

Fig. 3 Sharp Cone Geometry and Nomenclature

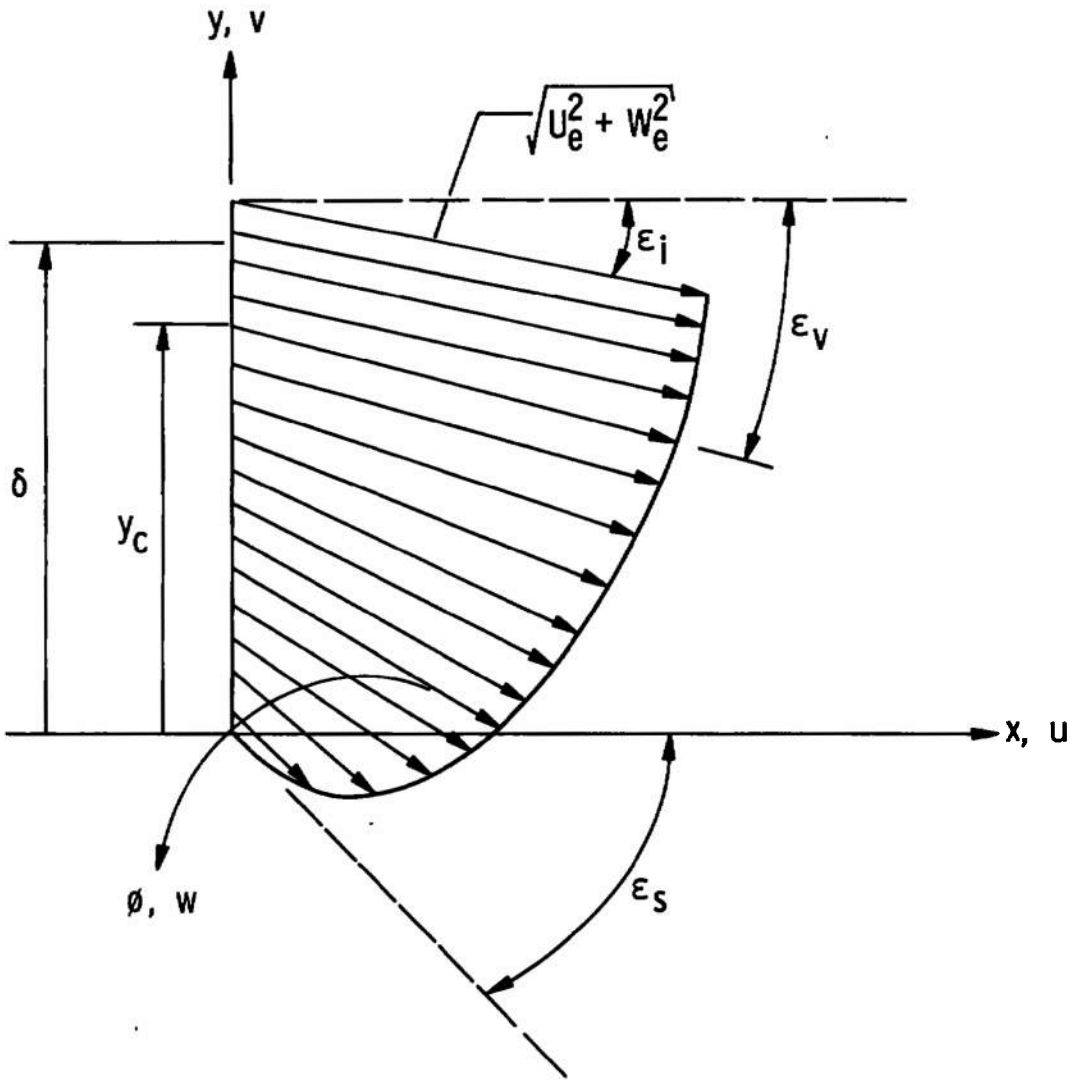

Fig. 4 Schematic of Three-Dimensional Boundary-Layer Velocity Profile in Body Coordinates Showing Definition of Upwash Angles

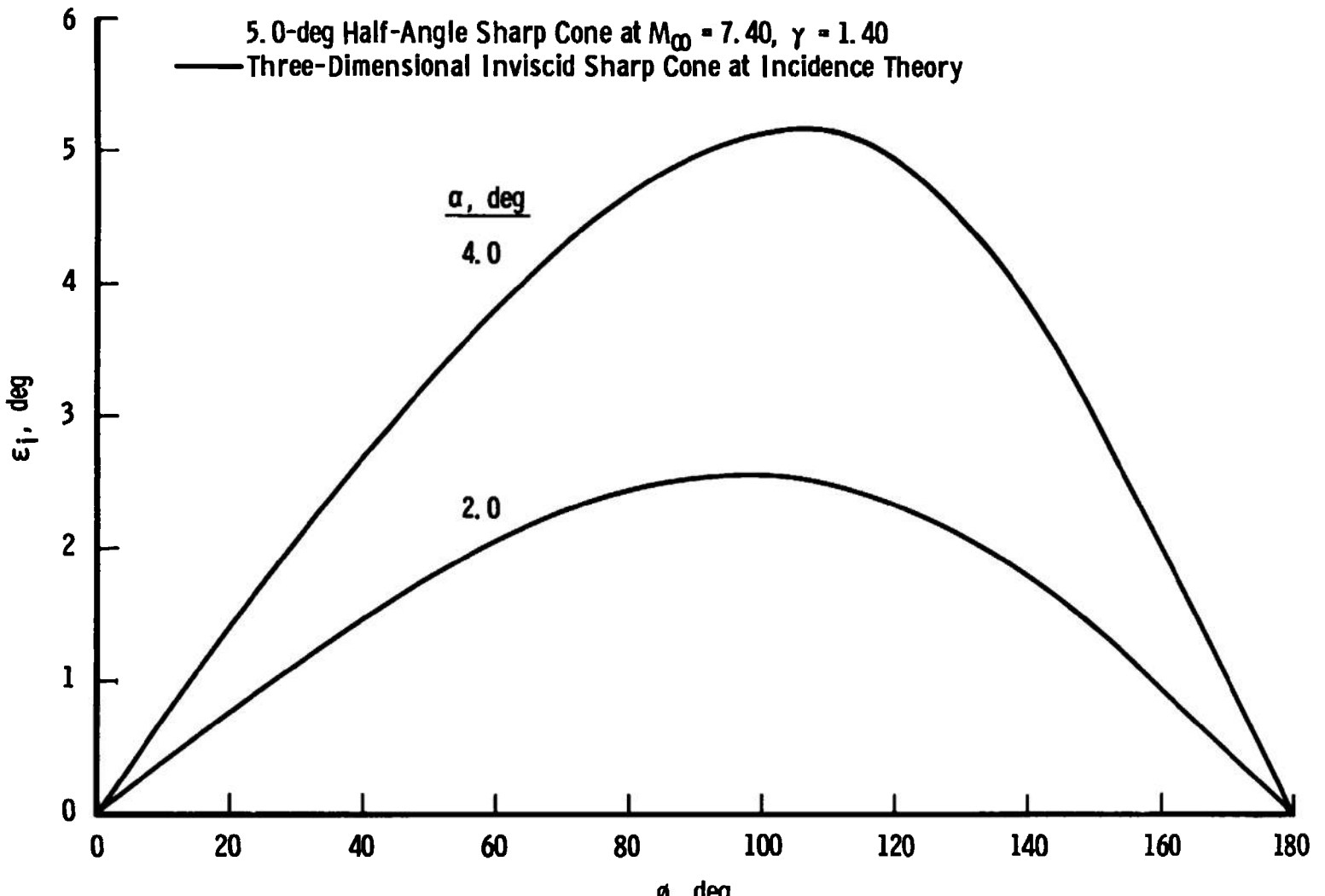

Fig. 5 Calculated Upwash Angles for Sharp Cones in Inviscid Flow

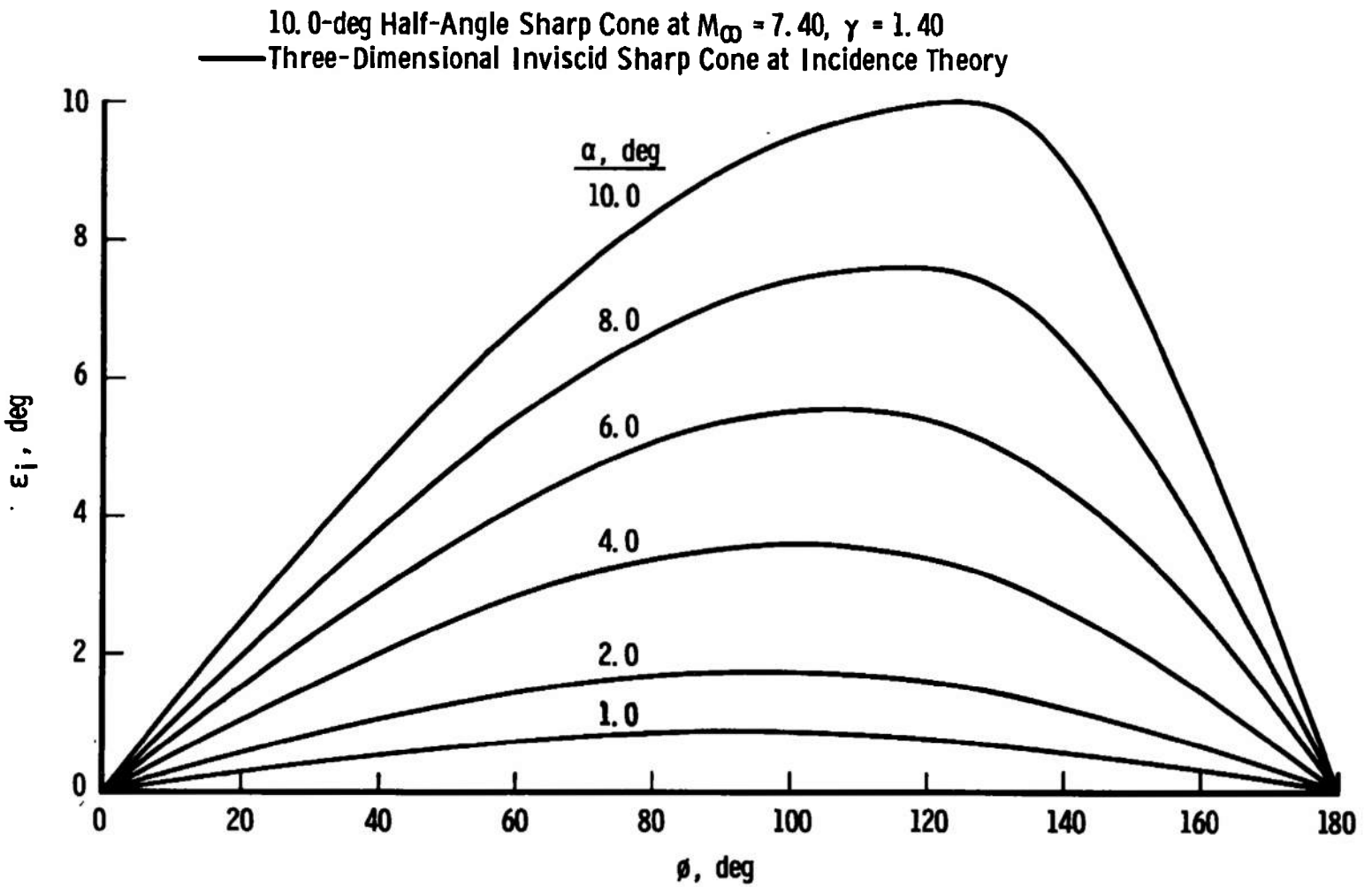

Fig. 5 Continued

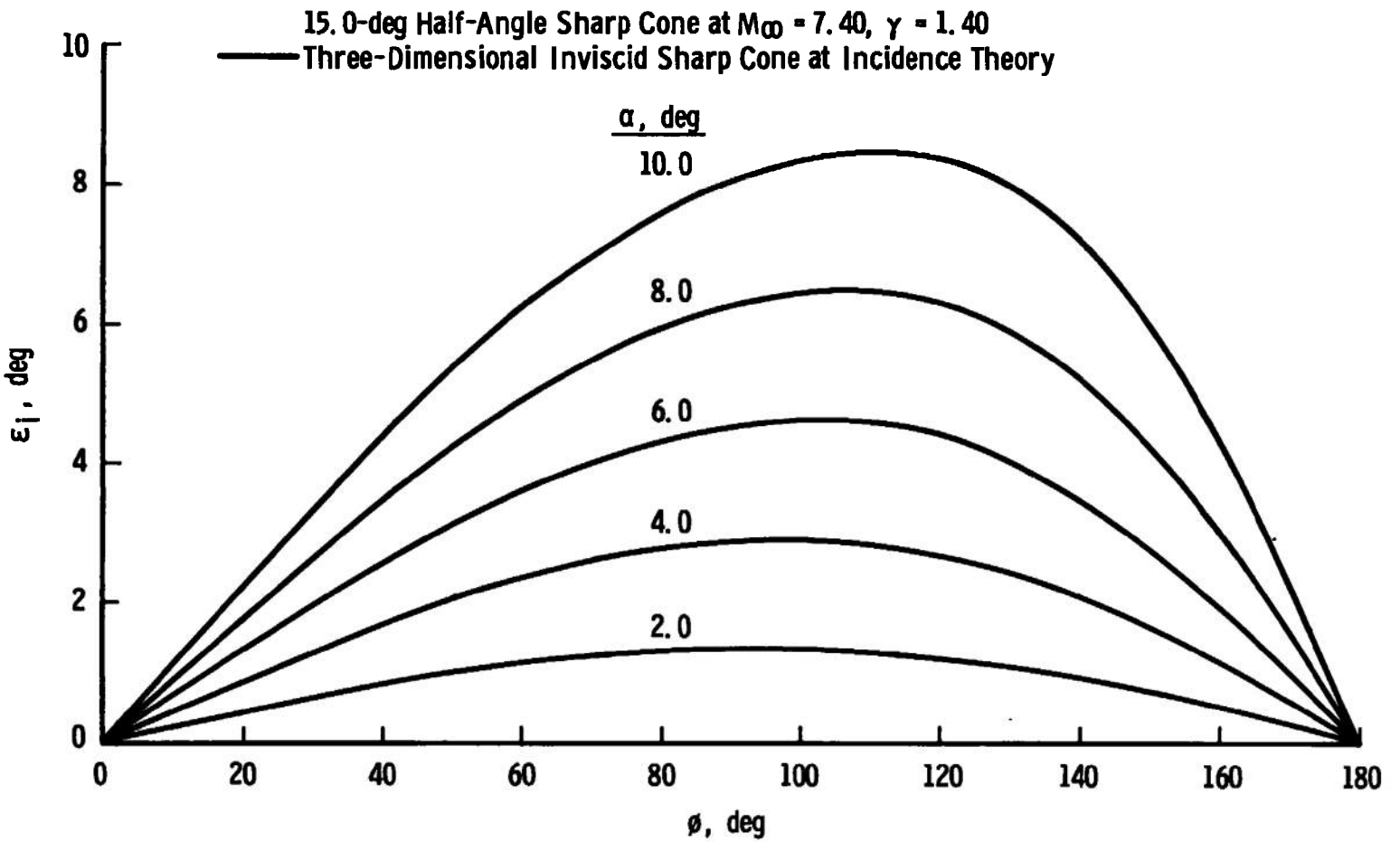

Fig. 5 Concluded

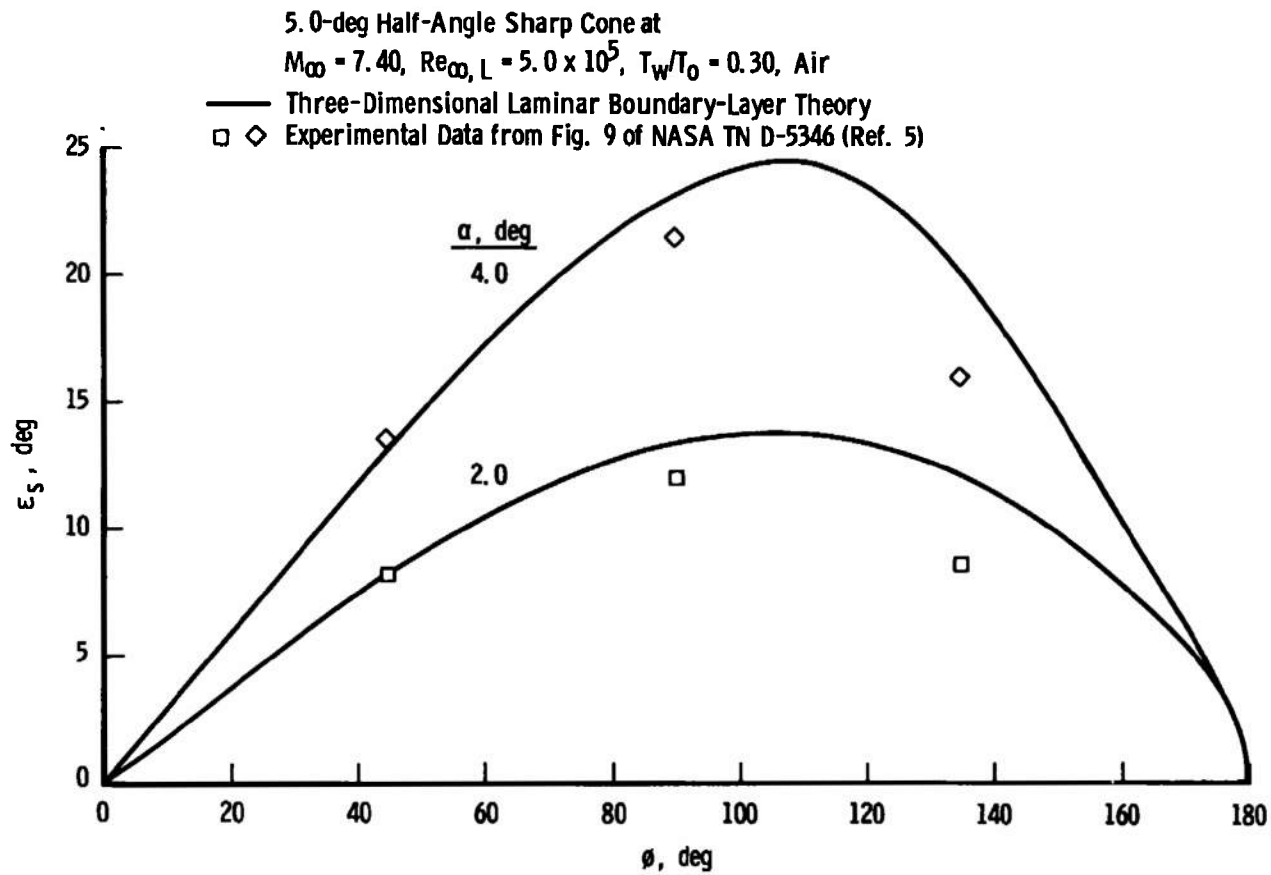

Fig. 6 Comparison of Calculated and Measured Surface Upwash Angles

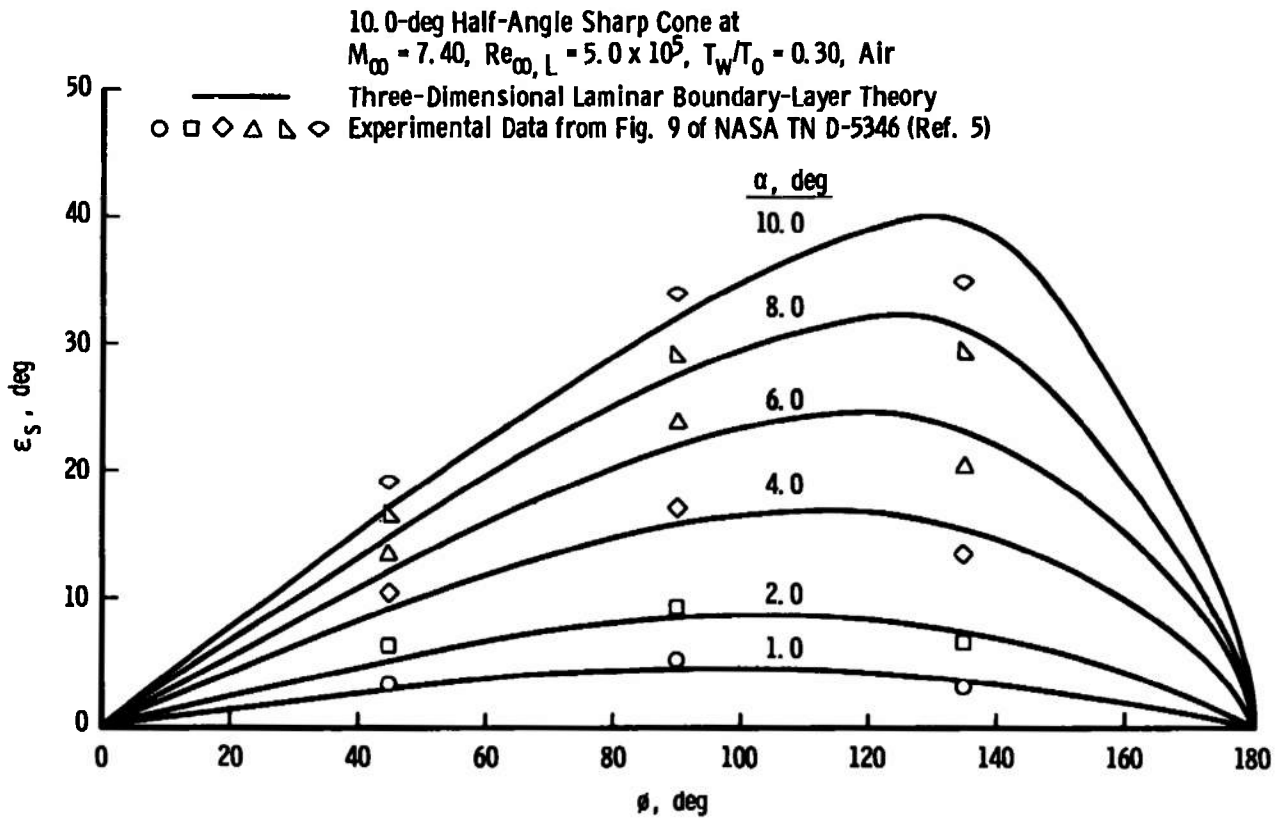

Fig. 6 Continued

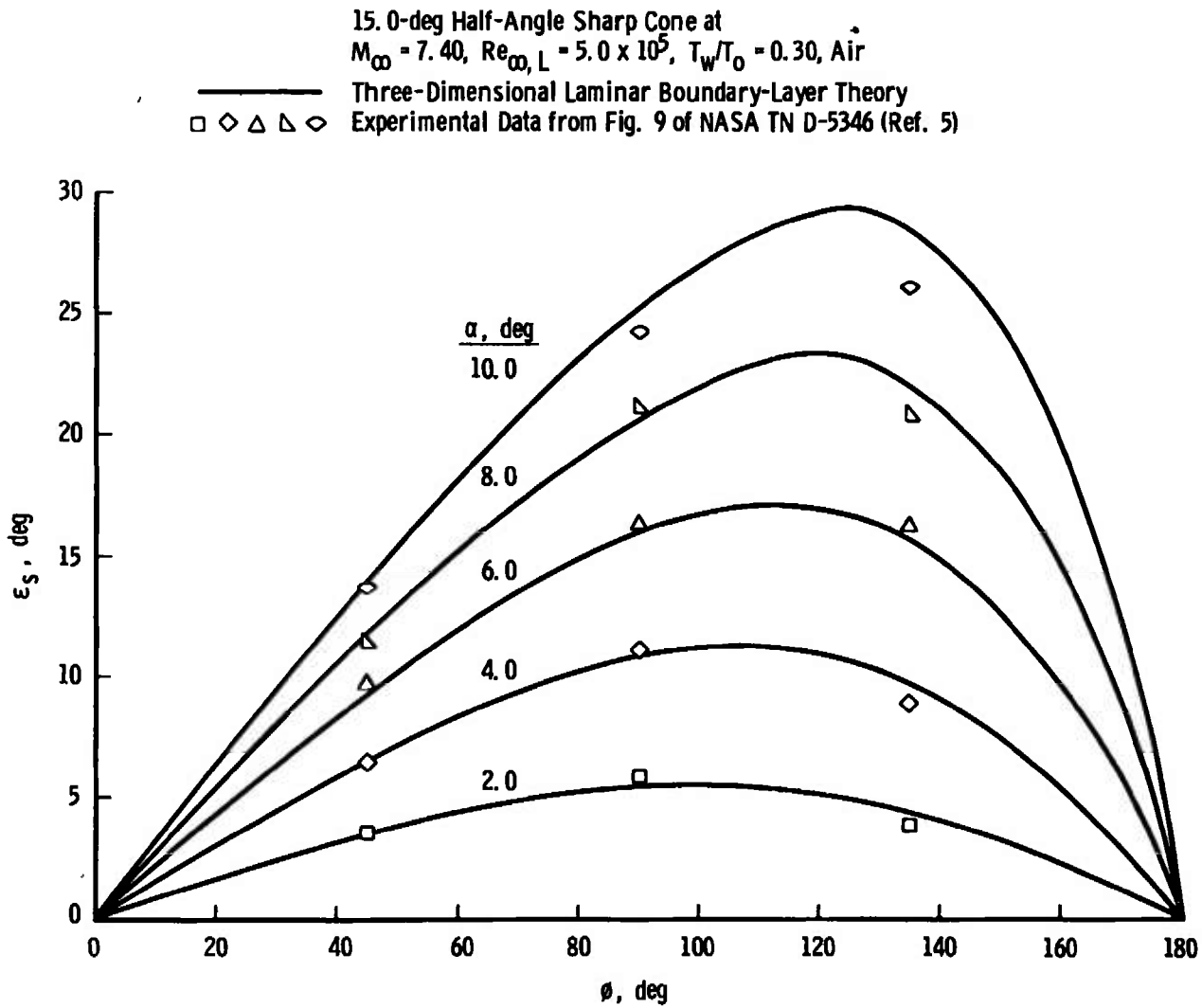

Fig. 6 Concluded

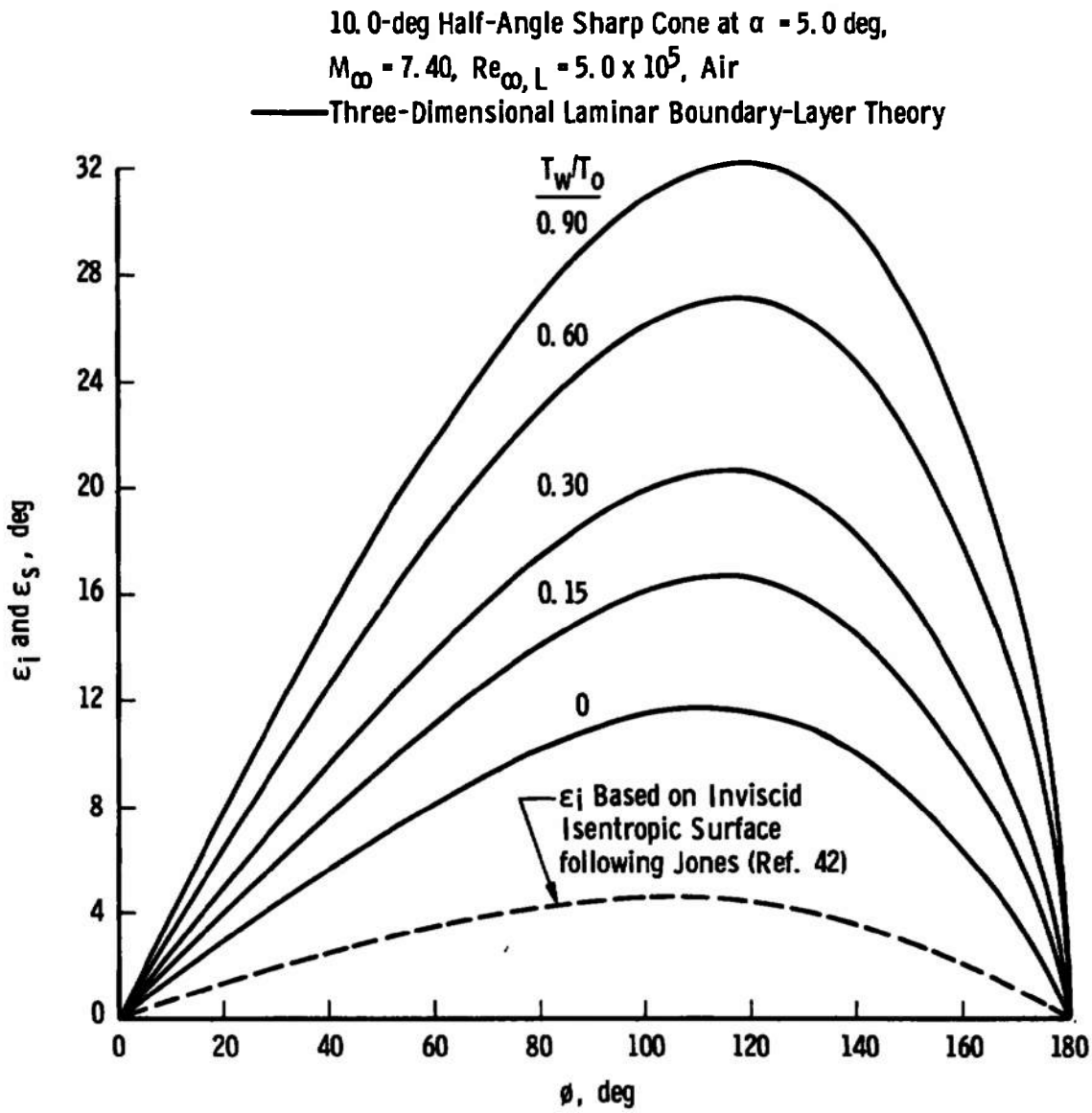

Fig. 7 Effects of Wall Temperature on Calculated Surface Upwash Angle

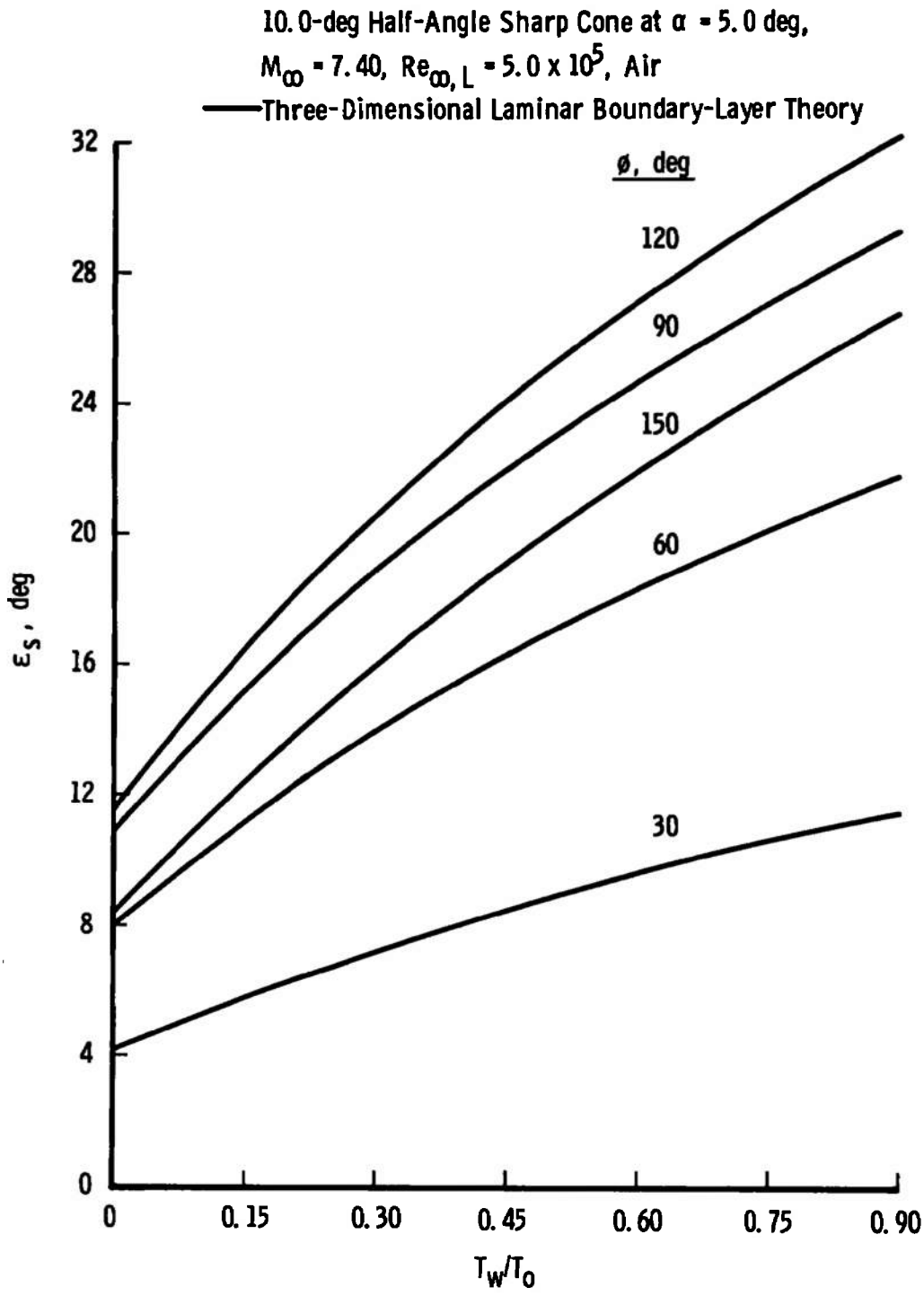

Fig. 8 Variation of Surface Upwash Angle with Wall Temperature at a Given Circumferential Location

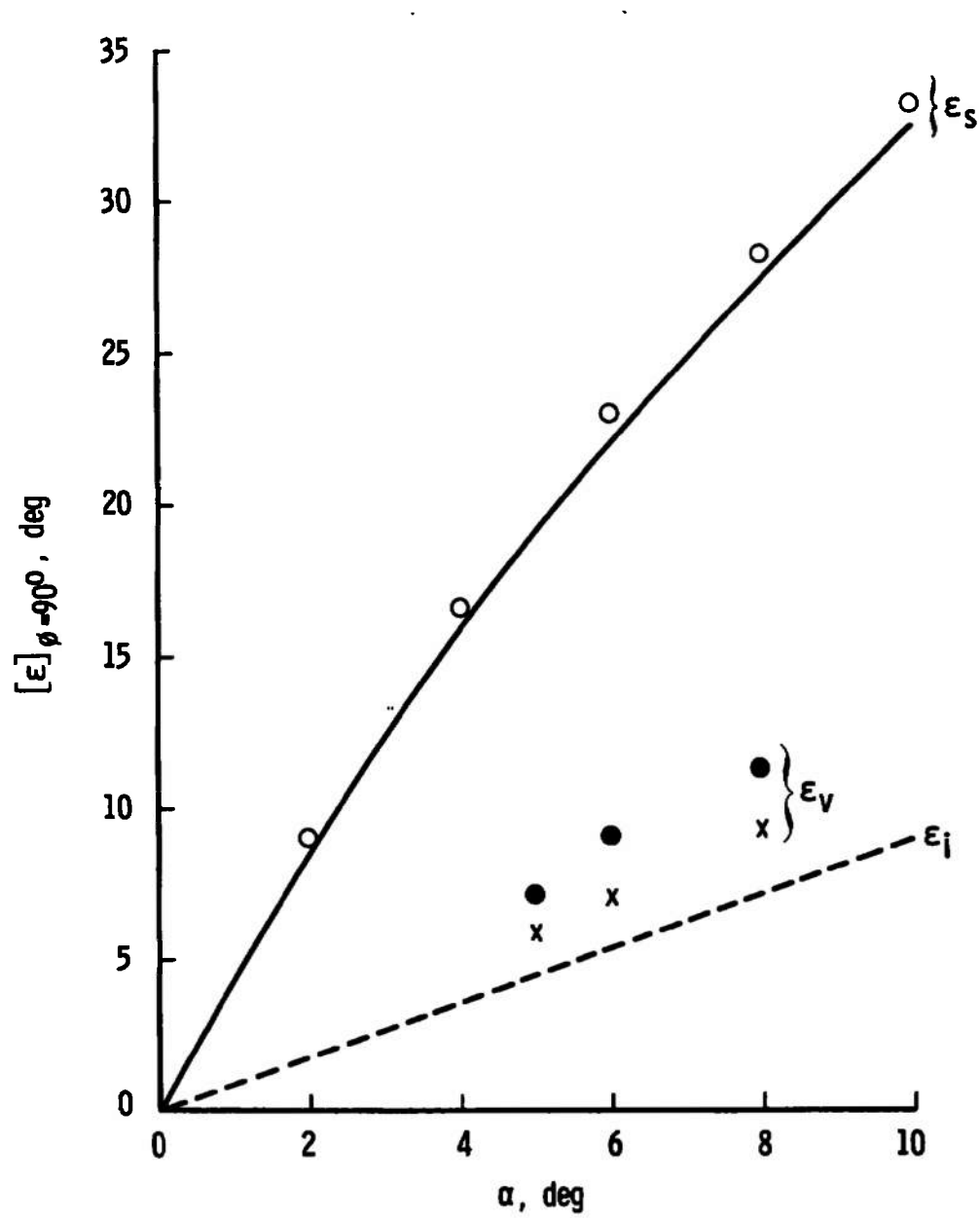

Fig. 9 Comparison of Calculated and Measured Vortex Angles at the Body Location ϕ = 90 deg

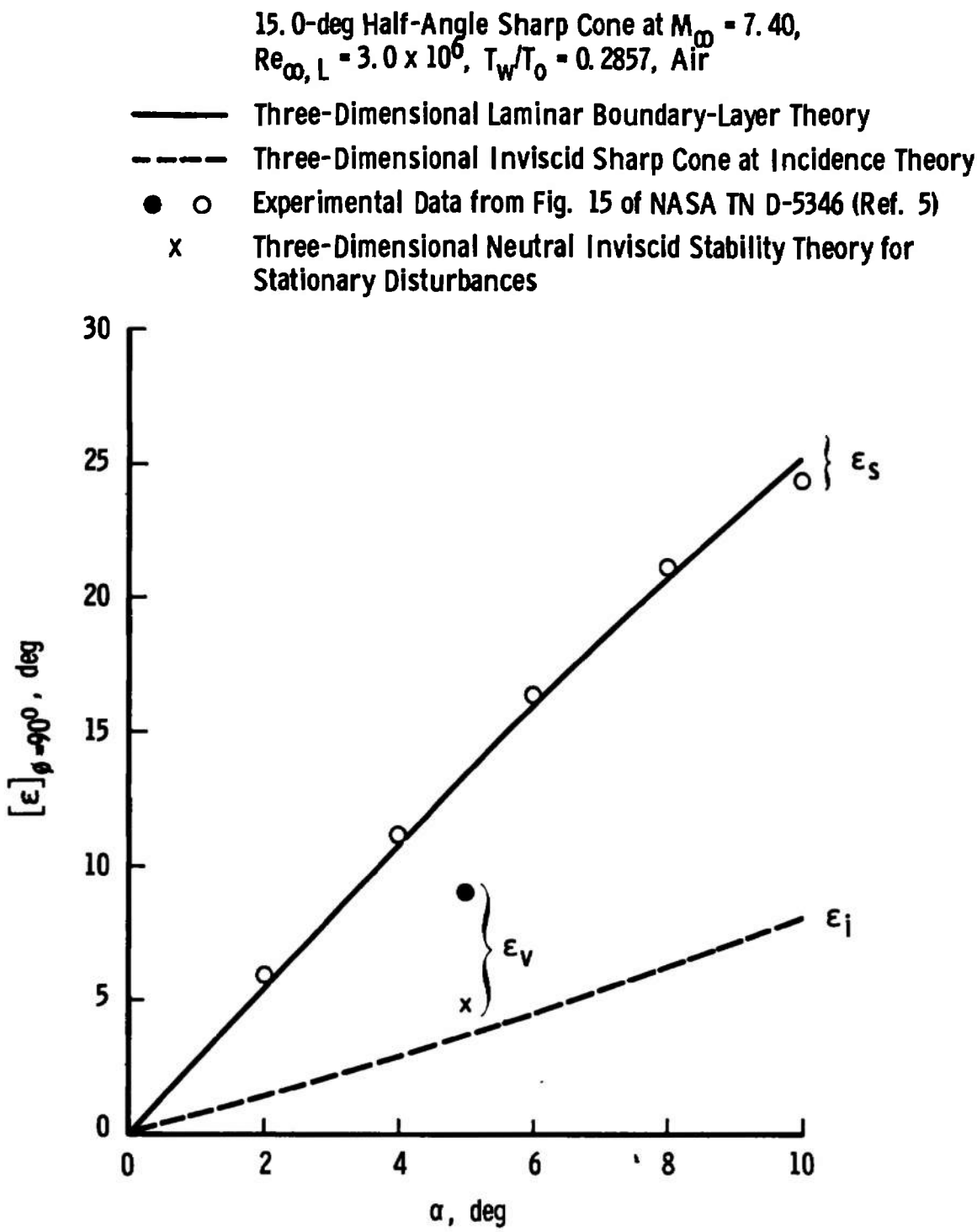

Fig. 9 Concluded

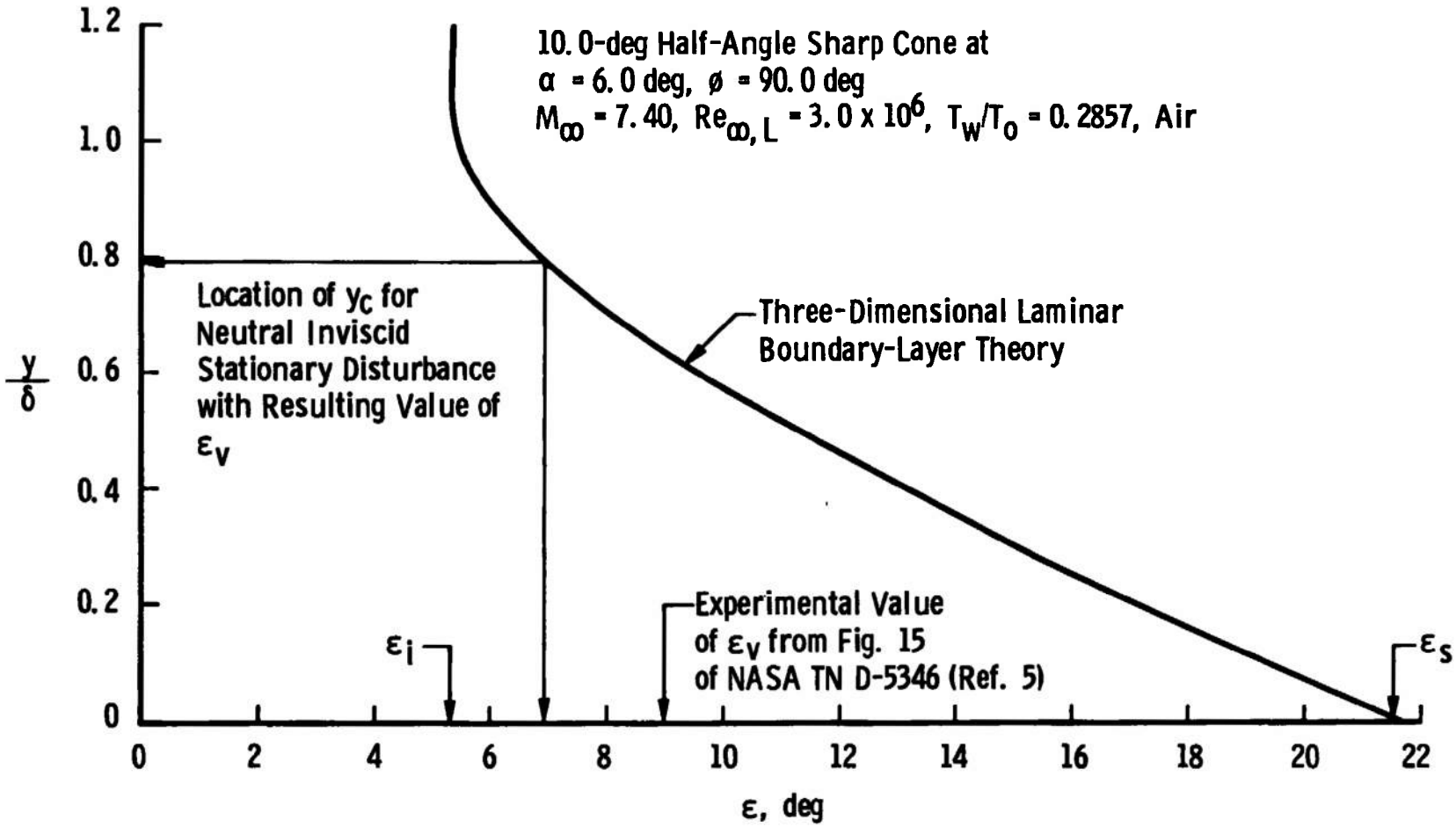

Fig. 10 Angular Turning of the Boundary-Layer Velocity Profile at the Body Location ϕ = 90 deg Including Position of Critical Height

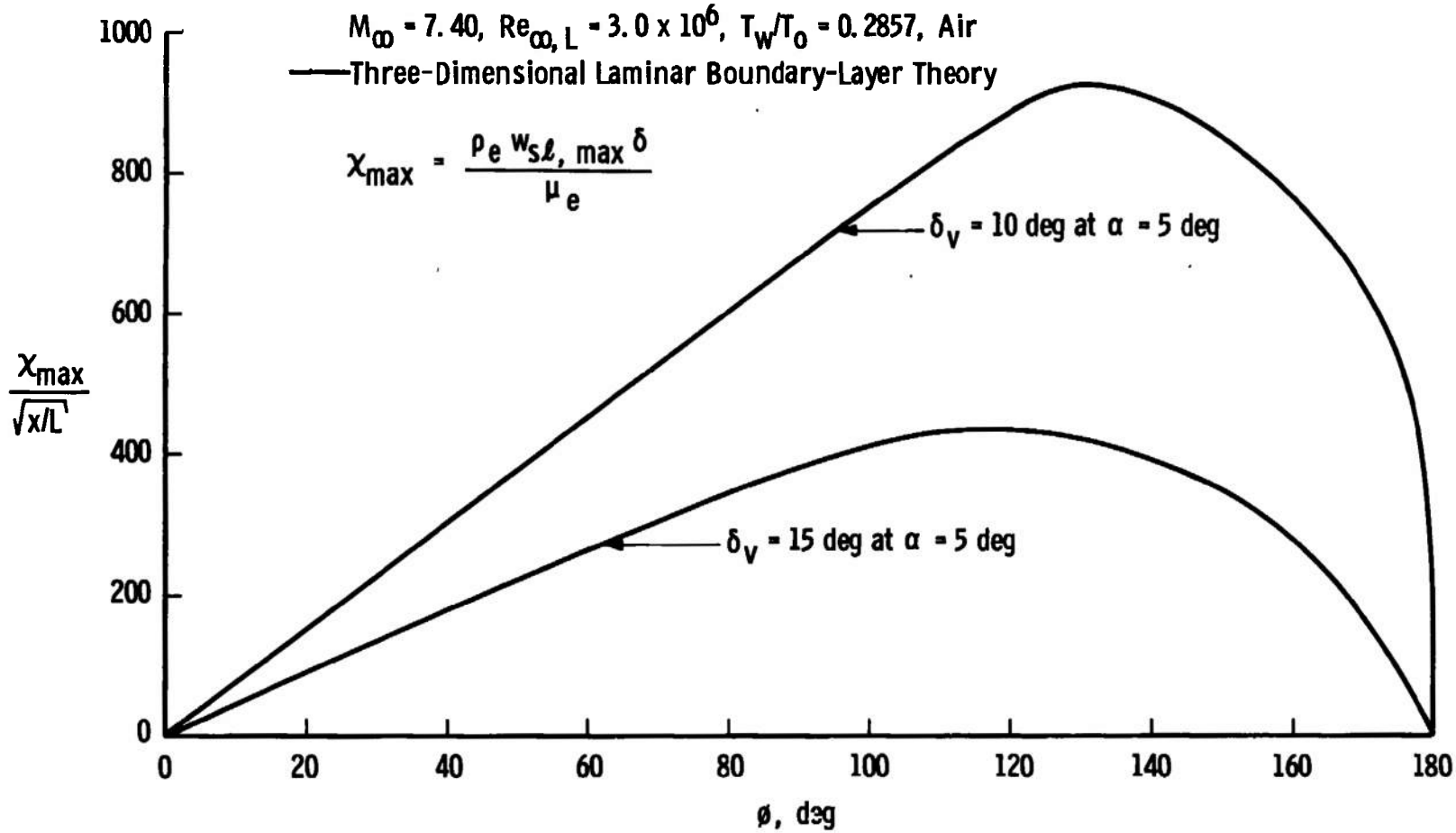

Fig. 11 Maximum Crossflow Reynolds Number Distribution

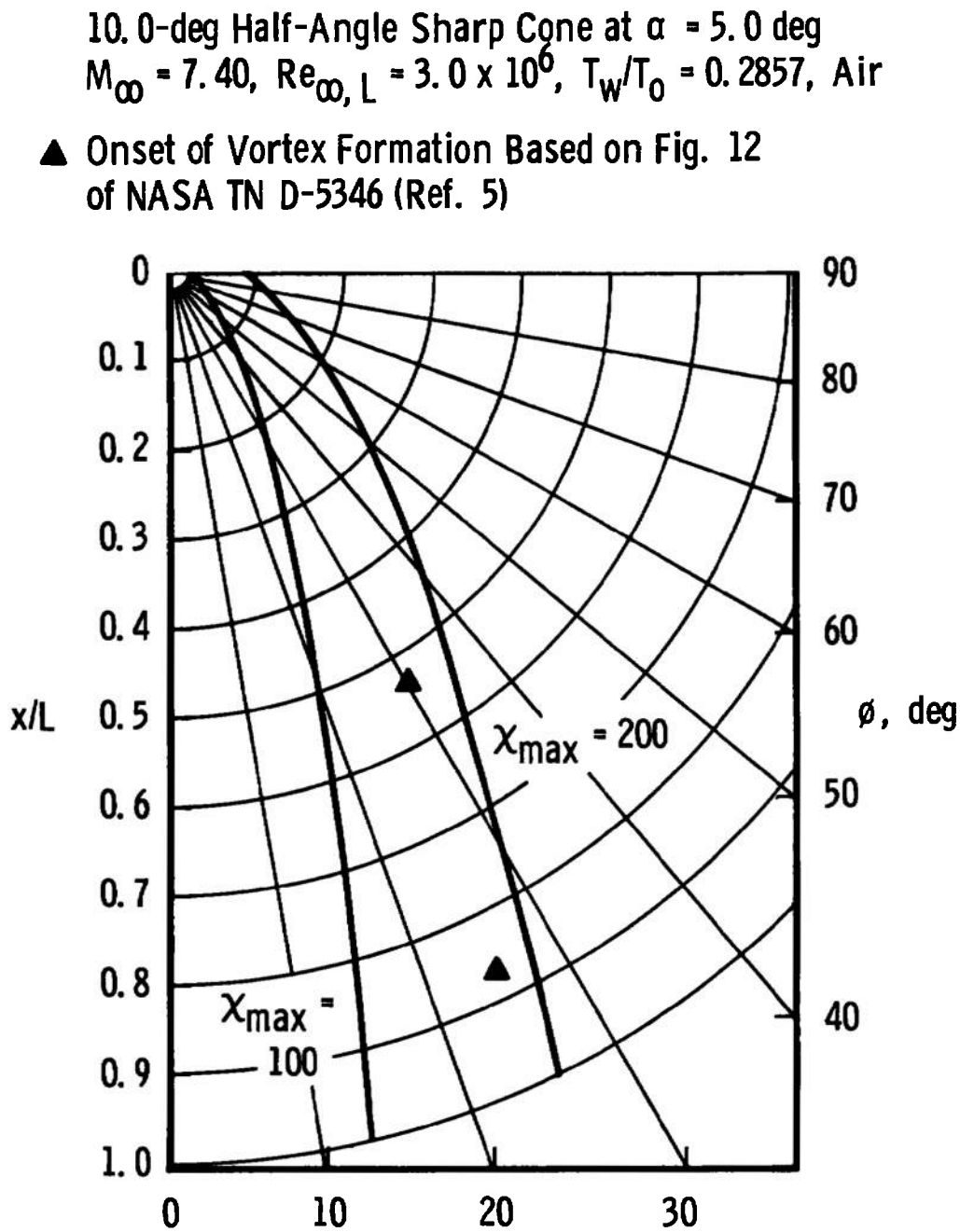

Fig. 12 Developed-Surface Plot Showing Onset to Vortex Formation Relative to Lines of Constant Maximum Crossflow Reynolds Number

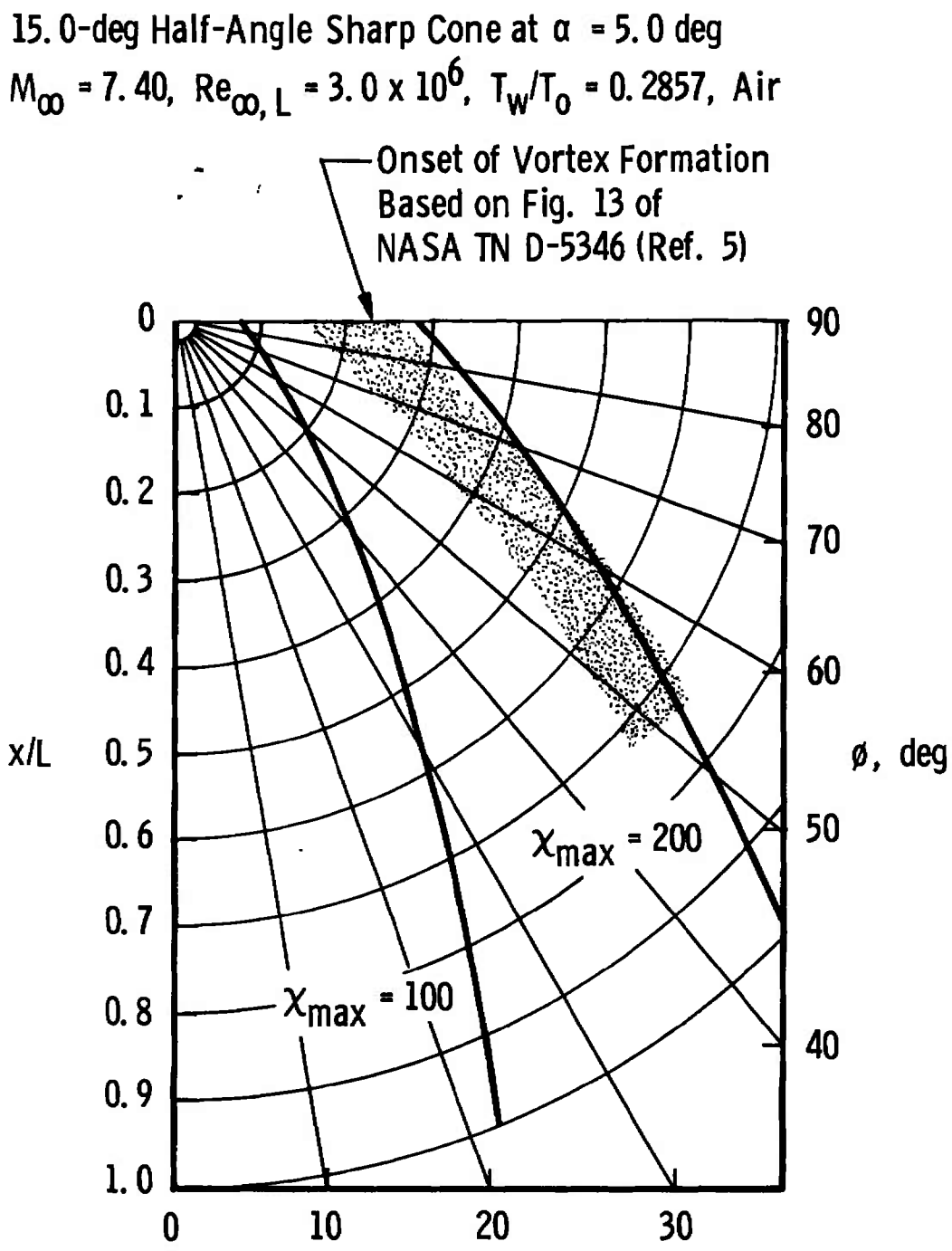

Fig. 12 Concluded

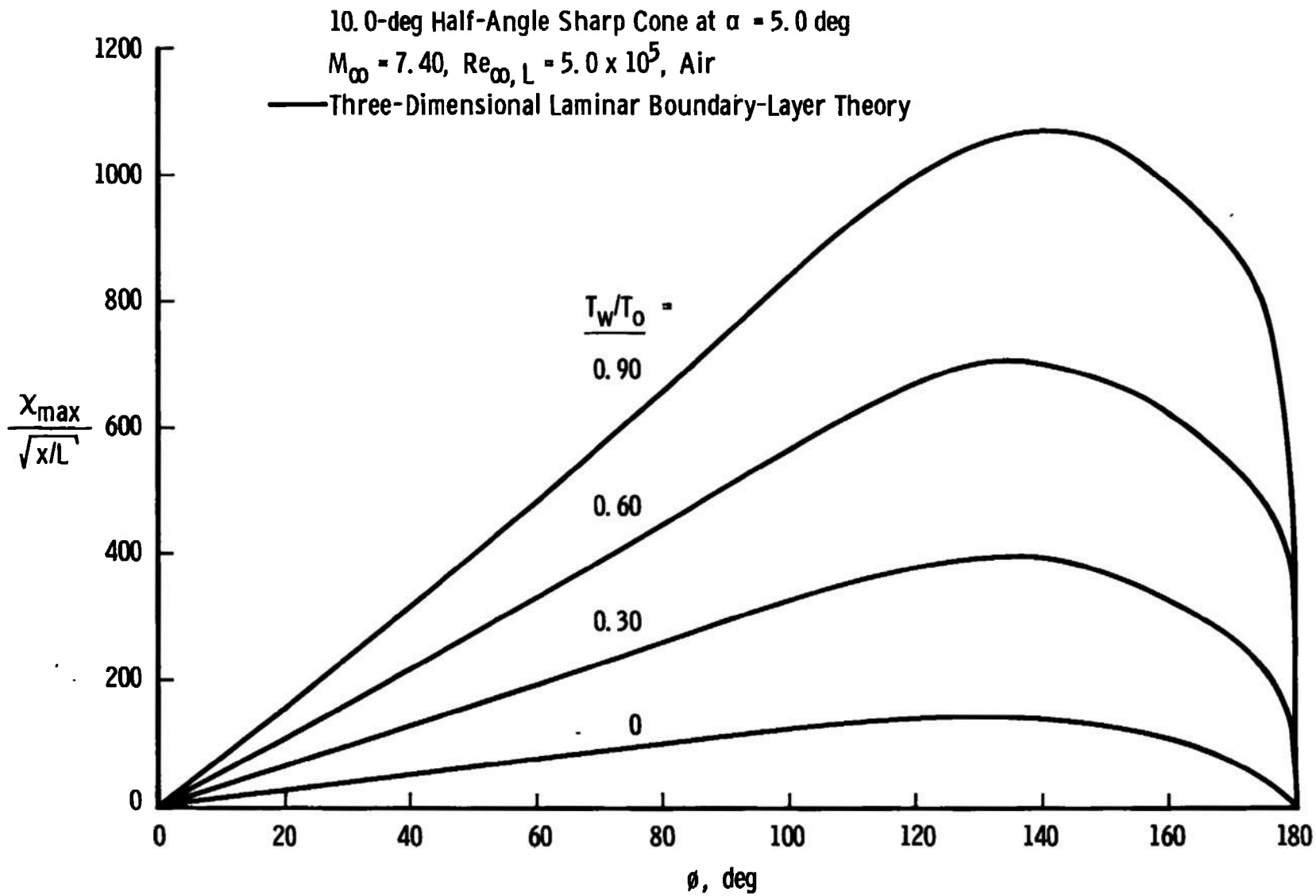

Fig. 13 Effects of Wall Temperature on Calculated Maximum Crossflow Reynolds Number Distribution

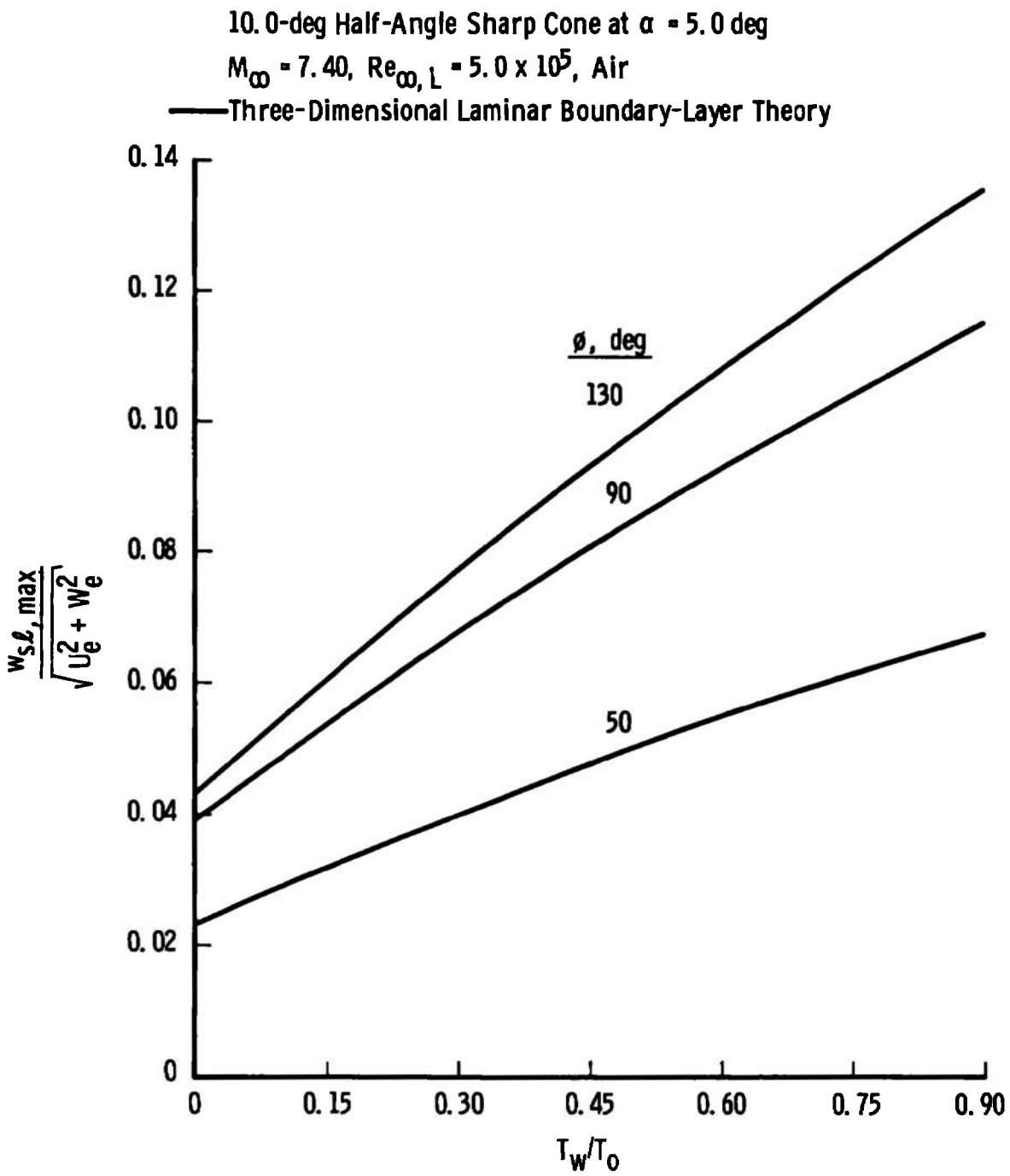

Fig. 14 Effects of Wall Temperature on Maximum Crossflow Velocity in Boundary Layer

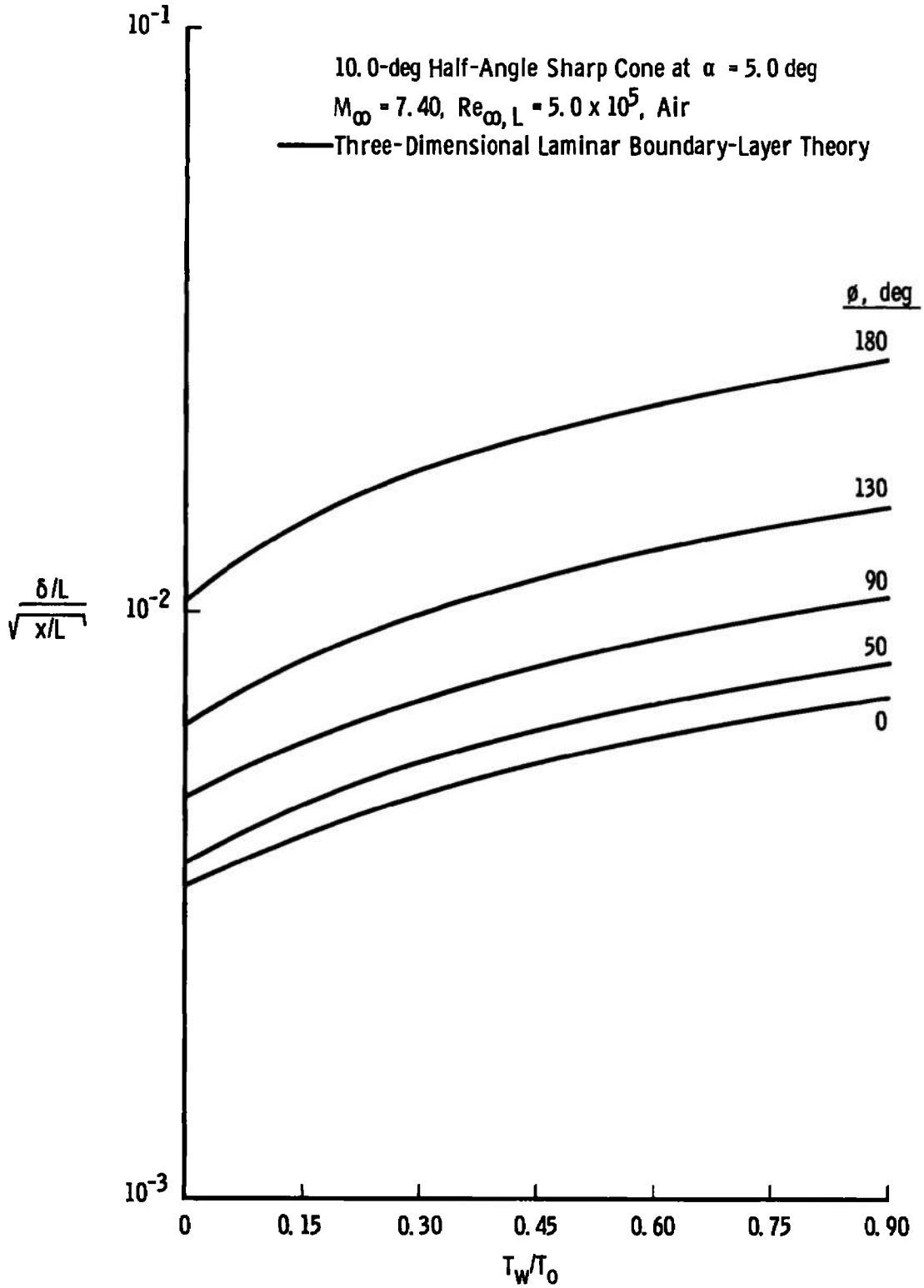

Fig. 15 Effects of Wall Temperature on Boundary-Layer Thickness

TABLE I
LAMINAR THREE-DIMENSIONAL BOUNDARY-LAYER PROFILES AT ϕ = 90 DEG FOR δ_v = 10 DEG AND α = 5 DEG

$\frac{y/L}{\sqrt{x/L}}$	u/U_e	w/W_e	T/T_e
0	0	0	2.068220E00
4.332620E-06	2.400000E-03	1.125000E-02	2.075740E 00
8.959950E-06	5.370000E-03	2.318000E-02	2.085800E 00
1.390330E-05	8.320000E-03	3.582000E-02	2.096420E 00
1.918540E-05	1.145000E-02	4.922000E-02	2.107630E 00
2.483110E-05	1.479000E-02	6.342000E-02	2.119450E 00
3.088700E-05	1.835000E-02	7.846000E-02	2.131920E 00
3.732170E-05	2.213000E-02	9.438000E-02	2.145060E 00
4.422640E-05	2.616000E-02	1.112300E-01	2.158900E 00
5.161460E-05	3.044000E-02	1.290700E-01	2.173450E 00
5.952230E-05	3.501000E-02	1.479300E-01	2.188760E 00
6.798860E-05	3.987000E-02	1.678800E-01	2.204830E 00
7.705580E-05	4.505000E-02	1.889500E-01	2.221700E 00
8.676950E-05	5.056000E-02	2.112200E-01	2.239390E 00
9.717850E-05	5.643000E-02	2.347200E-01	2.257900E 00
1.083370E-04	6.266000E-02	2.595100E-01	2.277260E 00
1.203020E-04	6.935000E-02	2.856400E-01	2.297470E 00
1.331360E-04	7.644000E-02	3.131700E-01	2.318540E 00
1.469050E-04	8.401000E-02	3.421400E-01	2.340470E 00
1.616820E-04	9.206000E-02	3.726000E-01	2.363230E 00
1.775440E-04	1.006500E-01	4.045400E-01	2.386820E 00
1.945760E-04	1.097900E-01	4.381500E-01	2.411190E 00
2.128680E-04	1.195400E-01	4.733100E-01	2.436300E 00
2.325170E-04	1.299200E-01	5.100500E-01	2.462090E 00
2.536250E-04	1.409900E-01	5.484400E-01	2.488470E 00
2.763060E-04	1.527600E-01	5.885100E-01	2.515340E 00
3.006750E-04	1.653300E-01	6.301400E-01	2.542570E 00
3.266600E-04	1.787100E-01	6.733300E-01	2.570000E 00
3.549930E-04	1.929500E-01	7.180200E-01	2.597430E 00
3.852140E-04	2.081200E-01	7.641200E-01	2.624630E 00
4.176720E-04	2.242500E-01	8.115100E-01	2.651330E 00
4.525170E-04	2.414100E-01	8.600200E-01	2.677180E 00
4.899090E-04	2.596500E-01	9.094700E-01	2.701820E 00
5.300080E-04	2.790300E-01	9.595900E-01	2.724410E 00
5.729780E-04	2.995500E-01	1.010040E 00	2.745620E 00
6.189800E-04	3.213500E-01	1.060600E 00	2.763690E 00
6.681760E-04	3.444800E-01	1.110700E 00	2.778360E 00
7.206970E-04	3.688400E-01	1.159920E 00	2.788920E 00
7.766960E-04	3.945600E-01	1.207690E 00	2.794570E 00
8.362820E-04	4.216100E-01	1.253400E 00	2.794450E 00
8.995440E-04	4.499900E-01	1.296360E 00	2.787670E 00
9.665360E-04	4.796500E-01	1.335450E 00	2.773280E 00
1.037270E-03	5.105600E-01	1.371090E 00	2.750370E 00
1.111710E-03	5.425900E-01	1.401310E 00	2.718050E 00
1.191760E-03	5.754000E-01	1.425740E 00	2.675530E 00
1.277240E-03	6.094000E-01	1.443670E 00	2.622210E 00
1.359940E-03	6.437700E-01	1.454500E 00	2.557680E 00
1.443530E-03	6.784100E-01	1.457760E 00	2.481880E 00
1.532640E-03	7.129900E-01	1.453200E 00	2.395140E 00
1.625820E-03	7.471200E-01	1.440410E 00	2.298220E 00
1.719570E-03	7.803400E-01	1.420400E 00	2.192400E 00
1.814370E-03	8.123300E-01	1.394070E 00	2.079460E 00
1.909700E-03	8.425400E-01	1.361270E 00	1.961620E 00
2.005080E-03	8.705900E-01	1.323750E 00	1.841520E 00
2.100070E-03	8.960800E-01	1.283020E 00	1.722010E 00
2.194370E-03	9.187400E-01	1.240750E 00	1.606030E 00
2.287820E-03	9.383600E-01	1.198490E 00	1.496410E 00
2.380420E-03	9.546400E-01	1.155520E 00	1.395680E 00
2.472370E-03	9.682100E-01	1.121750E 00	1.305660E 00
2.564069E-03	9.786400E-01	1.093360E 00	1.228400E 00
2.656070E-03	9.864000E-01	1.062730E 00	1.163980E 00
2.749150E-03	9.918400E-01	1.041540E 00	1.112580E 00
2.844140E-03	9.954300E-01	1.025790E 00	1.073420E 00
2.942010E-03	9.977000E-01	1.014470E 00	1.045130E 00
3.043720E-03	9.989400E-01	1.007570E 00	1.025910E 00
3.150190E-03	9.995700E-01	1.003780E 00	1.013740E 00
3.262290E-03	9.998500E-01	1.001610E 00	1.006630E 00
3.380820E-03	9.999600E-01	1.000490E 00	1.002470E 00
3.506470E-03	9.999900E-01	1.000190E 00	1.001090E 00
3.639870E-03	1.000000E 00	1.000050E 00	1.000350E 00
3.781600E-03	1.000000E 00	1.000010E 00	1.000090E 00
3.932240E-03	1.000000E 00	1.000000E 00	1.000020E 00
4.092350E-03	1.000000E 00	1.000000E 00	1.000000E 00
4.262560E-03	1.000000E 00	1.000000E 00	1.000000E 00
4.443080E-03	1.000000E 00	1.000000E 00	1.000000E 00
4.635910E-03	1.000000E 00	1.000000E 00	1.000000E 00
4.840250E-03	1.000000E 00	1.000000E 00	1.000000E 00
5.057570E-03	1.000000E 00	1.000000E 00	1.000000E 00
5.288580E-03	1.000000E 00	1.000000E 00	1.000000E 00
5.534150E-03	1.000000E 00	1.000000E 00	1.000000E 00
5.794190E-03	1.000000E 00	1.000000E 00	1.000000E 00
6.072670E-03	1.000000E 00	1.000000E 00	1.000000E 00
6.367630E-03	1.000000E 00	1.000000E 00	1.000000E 00
6.681120E-03	1.000000E 00	1.000000E 00	1.000000E 00
7.014420E-03	1.000000E 00	1.000000E 00	1.000000E 00

Inviscid Edge Quantities

U_e/V_∞ = 0.96685

W_e/V_∞ = 0.07493

p_e/p_∞ = 3.51520

$T_e/(V_\infty^2/R)$ = 0.02155

Free-Stream Conditions

M_∞ = 7.40 $Re_{\infty,L}$ = 3.0 x 10^6

Wall Temperature Ratio

T_w/T_0 = 0.28570

TABLE II
LAMINAR THREE-DIMENSIONAL BOUNDARY-LAYER PROFILES AT ϕ = 90 DEG FOR δ_v = 10 DEG AND α = 6 DEG

$\frac{y/L}{\sqrt{x/L}}$	u/U_e	w/W_e	T/T_e
0	0	0	2.023460E 00
4.362460E-06	2.630000E-03	1.194000E-02	2.032460E 00
9.021840E-06	5.430000E-03	2.243000E-02	2.042740E 00
1.399960E-05	8.410000E-03	3.527000E-02	2.052260E 00
1.931870E-05	1.159000E-02	4.847000E-02	2.064350E 00
2.590410E-05	1.496000E-02	6.244000E-02	2.075470E 00
3.108260E-05	1.855000E-02	7.724000E-02	2.088260E 00
3.752330E-05	2.237000E-02	9.231000E-02	2.101200E 00
4.453730E-05	2.644000E-02	1.095000E-01	2.114810E 00
5.198840E-05	3.078000E-02	1.270000E-01	2.129140E 00
5.994380E-05	3.540000E-02	1.456100E-01	2.144190E 00
6.847050E-05	4.031000E-02	1.652300E-01	2.159980E 00
7.760340E-05	4.554000E-02	1.859600E-01	2.176550E 00
8.738760E-05	5.112000E-02	2.074500E-01	2.193410E 00
9.787270E-05	5.706100E-02	2.309500E-01	2.212260E 00
1.091120E-04	6.338000E-02	2.553200E-01	2.231030E 00
1.211640E-04	7.012000E-02	2.815000E-01	2.250020E 00
1.340910E-04	7.724000E-02	3.090500E-01	2.271420E 00
1.479590E-04	8.494000E-02	3.365000E-01	2.292040E 00
1.628430E-04	9.309000E-02	3.664100E-01	2.315050E 00
1.788190E-04	1.017000E-01	3.978100E-01	2.338640E 00
1.959720E-04	1.110100E-01	4.307400E-01	2.361760E 00
2.143930E-04	1.208000E-01	4.652200E-01	2.386160E 00
2.341770E-04	1.313500E-01	5.012700E-01	2.411180E 00
2.554300E-04	1.425500E-01	5.389000E-01	2.436730E 00
2.782620E-04	1.544500E-01	5.781000E-01	2.462690E 00
3.027910E-04	1.671500E-01	6.188400E-01	2.488540E 00
3.291430E-04	1.806700E-01	6.610900E-01	2.515320E 00
3.574490E-04	1.950000E-01	7.047700E-01	2.541920E 00
3.878500E-04	2.103000E-01	7.494000E-01	2.567400E 00
4.204910E-04	2.266000E-01	7.960000E-01	2.593000E 00
4.555240E-04	2.440200E-01	8.433700E-01	2.617480E 00
4.931040E-04	2.624400E-01	8.915400E-01	2.640670E 00
5.333920E-04	2.820000E-01	9.403200E-01	2.662140E 00
5.765460E-04	3.027500E-01	9.894200E-01	2.681370E 00
6.227250E-04	3.247300E-01	1.038470E 00	2.697810E 00
6.720830E-04	3.480000E-01	1.087690E 00	2.710630E 00
7.247620E-04	3.725700E-01	1.136740E 00	2.719740E 00
7.808940E-04	3.984700E-01	1.185990E 00	2.723760E 00
8.405880E-04	4.257000E-01	1.225150E 00	2.722090E 00
9.039280E-04	4.542500E-01	1.266610E 00	2.713980E 00
9.709620E-04	4.840100E-01	1.304570E 00	2.694240E 00
1.041700E-03	5.151100E-01	1.338590E 00	2.674310E 00
1.116090E-03	5.472300E-01	1.367650E 00	2.641300E 00
1.194050E-03	5.803000E-01	1.391140E 00	2.594680E 00
1.275400E-03	6.141400E-01	1.408410E 00	2.545330E 00
1.359900E-03	6.484400E-01	1.418890E 00	2.491540E 00
1.447270E-03	6.830600E-01	1.422180E 00	2.407120E 00
1.537110E-03	7.175100E-01	1.418880E 00	2.322430E 00
1.629300E-03	7.514600E-01	1.406620E 00	2.228300E 00
1.722470E-03	7.844400E-01	1.388040E 00	2.126600E 00
1.817000E-03	8.161400E-01	1.363120E 00	2.017290E 00
1.912170E-03	8.460100E-01	1.332610E 00	1.904330E 00
2.007360E-03	8.736800E-01	1.297740E 00	1.794640E 00
2.102340E-03	8.987800E-01	1.259980E 00	1.675940E 00
2.196790E-03	9.210400E-01	1.220450E 00	1.565590E 00
2.290580E-03	9.402500E-01	1.181980E 00	1.462450E 00
2.383750E-03	9.563300E-01	1.144460E 00	1.367630E 00
2.476520E-03	9.693500E-01	1.111140E 00	1.283400E 00
2.569310E-03	9.794700E-01	1.081610E 00	1.211020E 00
2.662710E-03	9.869600E-01	1.057050E 00	1.151070E 00
2.757470E-03	9.922300E-01	1.037710E 00	1.103400E 00
2.854460E-03	9.957000E-01	1.023380E 00	1.067240E 00
2.954610E-03	9.978100E-01	1.013470E 00	1.041220E 00
3.058860E-03	9.990000E-01	1.007130E 00	1.023600E 00
3.168120E-03	9.995900E-01	1.003620E 00	1.012480E 00
3.283290E-03	9.998600E-01	1.001460E 00	1.006010E 00
3.405100E-03	9.999600E-01	1.000550E 00	1.002600E 00
3.534260E-03	9.999900E-01	1.000170E 00	1.000980E 00
3.671400E-03	1.000000E 00	1.000050E 00	1.000320E 00
3.817120E-03	1.000000E 00	1.000010E 00	1.000080E 00
3.972000E-03	1.000000E 00	1.000000E 00	1.000020E 00
4.136620E-03	1.000000E 00	1.000000E 00	1.000000E 00
4.311620E-03	1.000000E 00	1.000000E 00	1.000000E 00
4.497640E-03	1.000000E 00	1.000000E 00	1.000000E 00
4.695370E-03	1.000000E 00	1.000000E 00	1.000000E 00
4.905570E-03	1.000000E 00	1.000000E 00	1.000000E 00
5.129010E-03	1.000000E 00	1.000000E 00	1.000000E 00
5.366520E-03	1.000000E 00	1.000000E 00	1.000000E 00
5.619000E-03	1.000000E 00	1.000000E 00	1.000000E 00
5.887390E-03	1.000000E 00	1.000000E 00	1.000000E 00
6.172680E-03	1.000000E 00	1.000000E 00	1.000000E 00
6.475940E-03	1.000000E 00	1.000000E 00	1.000000E 00
6.798320E-03	1.000000E 00	1.000000E 00	1.000000E 00
7.141000E-03	1.000000E 00	1.000000E 00	1.000000E 00

Inviscid Edge Quantities

U_e/V_∞ = 0.96389

W_e/V_∞ = 0.09010

p_e/p_∞ = 8.46740

$T_e/(V_\infty^2/R)$ = 0.02201

Free-Stream Conditions

M_∞ = 7.40, $Re_{\infty,L}$ = 3.0 x 10^6

Wall Temperature Ratio

T_w/T_o = 0.28570

TABLE III
LAMINAR THREE-DIMENSIONAL BOUNDARY-LAYER PROFILES AT ϕ = 90 DEG FOR δ_v = 10 DEG AND α = 8 DEG

$y/\sqrt{x/L}$	u/U_e	w/W_e	T/T_e
0	0	0	.034180E 00
4.421820E-06	2.680000E-03	1.041000E-02	1.943260E 00
9.144830E-06	5.520000E-03	2.026000E-02	1.952440E 00
1.419600E-05	8.550000E-03	3.443000E-02	1.962940E 00
1.958300E-05	1.176000E-02	4.726000E-02	1.973600E 00
2.534690E-05	1.521000E-02	6.080000E-02	1.984820E 00
3.150950E-05	1.887000E-02	7.530000E-02	1.996650E 00
3.810030E-05	2.276000E-02	9.057000E-02	2.009090E 00
4.516090E-05	2.690000E-02	1.067000E-01	2.022150E 00
5.269560E-05	3.131000E-02	1.238100E-01	2.035690E 00
6.077120E-05	3.600000E-02	1.418000E-01	2.050310E 00
6.941760E-05	4.100000E-02	1.607000E-01	2.065620E 00
7.867720E-05	4.633000E-02	1.811000E-01	2.081240E 00
8.859820E-05	5.200000E-02	2.026700E-01	2.097790E 00
9.922910E-05	5.804000E-02	2.248700E-01	2.115080E 00
1.106240E-04	6.447000E-02	2.485400E-01	2.133100E 00
1.226420E-04	7.132000E-02	2.734400E-01	2.151870E 00
1.359460E-04	7.862000E-02	2.997200E-01	2.171370E 00
1.500040E-04	8.640000E-02	3.273100E-01	2.191600E 00
1.650880E-04	9.469000E-02	3.563000E-01	2.212520E 00
1.812770E-04	1.035100E-01	3.867000E-01	2.233120E 00
1.986550E-04	1.129200E-01	4.185400E-01	2.254330E 00
2.173140E-04	1.229400E-01	4.518400E-01	2.279120E 00
2.372490E-04	1.336100E-01	4.867000E-01	2.302350E 00
2.584650E-04	1.449400E-01	5.225000E-01	2.326060E 00
2.819710E-04	1.571000E-01	5.607500E-01	2.350020E 00
3.067860E-04	1.700000E-01	5.999400E-01	2.374120E 00
3.334330E-04	1.837000E-01	6.405500E-01	2.398200E 00
3.620440E-04	1.983400E-01	6.824000E-01	2.422070E 00
3.927950E-04	2.137100E-01	7.256000E-01	2.445480E 00
4.257100E-04	2.304400E-01	7.698500E-01	2.468160E 00
4.610500E-04	2.480500E-01	8.150100E-01	2.489610E 00
4.988500E-04	2.667300E-01	8.609100E-01	2.510060E 00
5.395400E-04	2.866600E-01	9.072400E-01	2.528490E 00
5.826840E-04	3.075800E-01	9.538400E-01	2.544630E 00
6.294340E-04	3.298500E-01	1.000320E 00	2.557980E 00
6.798350E-04	3.533600E-01	1.046230E 00	2.569430E 00
7.315240E-04	3.782200E-01	1.091400E 00	2.573870E 00
7.882240E-04	4.043700E-01	1.134510E 00	2.575110E 00
8.486370E-04	4.318400E-01	1.176400E 00	2.576930E 00
9.116380E-04	4.606000E-01	1.214400E 00	2.566500E 00
9.784710E-04	4.906000E-01	1.250300E 00	2.543300E 00
1.049140E-03	5.217700E-01	1.282030E 00	2.518370E 00
1.123390E-03	5.535500E-01	1.309140E 00	2.485120E 00
1.201140E-03	5.871100E-01	1.331400E 00	2.442490E 00
1.282210E-03	6.209500E-01	1.347330E 00	2.391570E 00
1.366390E-03	6.551700E-01	1.357400E 00	2.330710E 00
1.453390E-03	6.895700E-01	1.360990E 00	2.260490E 00
1.542860E-03	7.237400E-01	1.357950E 00	2.181360E 00
1.634410E-03	7.574000E-01	1.348350E 00	2.094150E 00
1.727550E-03	7.900000E-01	1.332520E 00	2.000100E 00
1.821970E-03	8.216300E-01	1.311040E 00	1.900430E 00
1.917110E-03	8.505500E-01	1.284730E 00	1.794840E 00
2.012620E-03	8.771300E-01	1.254500E 00	1.684440E 00
2.108160E-03	9.022400E-01	1.222140E 00	1.572190E 00
2.203550E-03	9.239400E-01	1.188560E 00	1.458400E 00
2.298710E-03	9.425400E-01	1.155140E 00	1.342300E 00
2.392730E-03	9.581400E-01	1.123170E 00	1.319170E 00
2.486880E-03	9.707100E-01	1.094560E 00	1.245180E 00
2.584620E-03	9.804400E-01	1.069260E 00	1.191930E 00
2.681550E-03	9.875100E-01	1.048400E 00	1.129800E 00
2.780420E-03	9.925100E-01	1.031450E 00	1.048720E 00
2.882100E-03	9.959100E-01	1.019450E 00	1.057430E 00
2.987490E-03	9.979100E-01	1.011450E 00	1.035130E 00
3.097520E-03	9.990500E-01	1.006500E 00	1.020450E 00
3.213080E-03	9.995100E-01	1.002400E 00	1.010520E 00
3.335020E-03	9.994400E-01	1.001270E 00	1.005130E 00
3.464110E-03	9.994000E-01	1.000480E 00	1.002220E 00
3.601030E-03	9.999500E-01	1.000160E 00	1.000950E 00
3.744440E-03	1.000000E 00	1.000040E 00	1.000260E 00
3.893960E-03	1.000000E 00	1.000010E 00	1.000080E 00
4.065180E-03	1.000000E 00	1.000000E 00	1.000020E 00
4.239740E-03	1.000000E 00	1.000000E 00	1.000000E 00
4.425300E-03	1.000000E 00	1.000100E 00	1.000000E 00
4.425500E-03	1.000000E 00	1.000000E 00	1.000000E 00
4.832220E-03	1.000000E 00	1.000000E 00	1.000000E 00
5.256110E-03	1.000000E 00	1.000000E 00	1.000000E 00
5.292040E-03	1.000000E 00	1.000000E 00	1.000000E 00
5.541890E-03	1.000000E 00	1.000000E 00	1.000000E 00
5.811610E-03	1.000000E 00	1.000000E 00	1.000000E 00
6.096200E-03	1.000000E 00	1.000000E 00	1.000000E 00
6.394710E-03	1.000000E 00	1.000000E 00	1.000000E 00
6.702490E-03	1.000000E 00	1.000000E 00	1.000000E 00
7.052120E-03	1.000000E 00	1.000000E 00	1.000000E 00
7.425490E-03	1.000000E 00	1.000000E 00	1.000000E 00

Inviscid Edge Quantities

U_e/V_∞ = 0.85692

W_e/V_∞ = 0.12003

P_e/P_∞ = 3.47510

$T_e/(V_\infty^2/R)$ = 0.02306

Free-Stream Conditions

M_∞ = 7.00 $Re_{\infty,L}$ = 3.0 x 10^6

Wall Temperature Ratio

T_w/T_{t_2} = 0.28570

TABLE IV
LAMINAR THREE-DIMENSIONAL BOUNDARY-LAYER PROFILES AT ϕ = 90 DEG FOR δ_v = 15 DEG AND α = 5 DEG

$y/L \sqrt{x/L}$	u/U_e	w/W_e	T/T_e
0	0	0	1.498070E 00
3.194780E-04	2.120400E-03	4.790000E-03	1.504600E 00
8.606030E-04	4.097000E-03	1.011000E-02	1.511000E 00
1.024930E-05	7.720000E-03	2.000000E-02	1.518000E 00
1.414120E-05	1.063000E-02	3.640000E-02	1.526500E 00
1.830000E-05	1.373000E-02	4.950000E-02	1.534600E 00
2.274490E-05	1.703000E-02	6.137000E-02	1.543300E 00
2.749710E-05	2.054000E-02	7.385000E-02	1.552400E 00
3.257920E-05	2.427000E-02	8.707000E-02	1.562000E 00
3.801570E-05	2.825000E-02	1.010700E-01	1.572120E 00
4.383300E-05	3.243000E-02	1.150000E-01	1.582700E 00
5.005970E-05	3.700000E-02	1.315700E-01	1.594030E 00
5.672670E-05	4.180000E-02	1.491000E-01	1.605450E 00
6.386750E-05	4.691000E-02	1.657100E-01	1.617820E 00
7.151820E-05	5.236000E-02	1.842500E-01	1.631350E 00
7.971790E-05	5.816000E-02	2.034400E-01	1.645350E 00
8.857890E-05	6.434000E-02	2.246200E-01	1.659430E 00
9.793690E-05	7.092000E-02	2.463000E-01	1.674470E 00
1.086510E-04	7.797000E-02	2.693000E-01	1.690210E 00
1.189060E-04	8.541000E-02	2.939000E-01	1.706630E 00
1.305580E-04	9.337000E-02	3.191100E-01	1.723760E 00
1.430710E-04	1.018000E-01	3.459400E-01	1.741570E 00
1.568110E-04	1.108000E-01	3.741000E-01	1.760070E 00
1.709510E-04	1.205000E-01	4.037000E-01	1.779200E 00
1.854700E-04	1.302000E-01	4.344000E-01	1.799000E 00
2.031520E-04	1.417400E-01	4.671100E-01	1.819370E 00
2.210870E-04	1.534000E-01	5.009700E-01	1.840270E 00
2.403730E-04	1.658200E-01	5.362000E-01	1.861300E 00
2.611110E-04	1.790000E-01	5.729000E-01	1.883350E 00
2.834140E-04	1.931600E-01	6.110000E-01	1.905320E 00
3.073970E-04	2.081200E-01	6.505000E-01	1.927390E 00
3.231840E-04	2.241000E-01	6.911000E-01	1.949000E 00
3.600050E-04	2.411000E-01	7.329000E-01	1.971130E 00
3.906950E-04	2.592000E-01	7.757000E-01	1.992230E 00
4.228950E-04	2.785000E-01	8.193000E-01	2.012700E 00
4.576470E-04	2.989500E-01	8.636000E-01	2.031990E 00
4.934970E-04	3.206200E-01	9.079000E-01	2.049710E 00
5.333900E-04	3.435900E-01	9.524000E-01	2.065450E 00
5.756670E-04	3.678000E-01	9.964000E-01	2.078720E 00
6.208620E-04	3.935400E-01	1.039100E 00	2.088460E 00
6.690900E-04	4.205700E-01	1.081500E 00	2.095560E 00
7.204840E-04	4.489700E-01	1.121370E 00	2.097870E 00
7.751010E-04	4.787100E-01	1.159700E 00	2.095210E 00
8.330070E-04	5.097400E-01	1.193120E 00	2.086660E 00
8.942220E-04	5.419400E-01	1.223420E 00	2.072160E 00
9.587239E-04	5.752400E-01	1.243320E 00	2.050460E 00
1.026440E-03	6.093300E-01	1.273370E 00	2.021240E 00
1.097250E-03	6.441000E-01	1.285110E 00	1.984130E 00
1.170980E-03	6.793200E-01	1.294000E 00	1.938560E 00
1.247390E-03	7.144500E-01	1.296440E 00	1.885860E 00
1.326200E-03	7.491700E-01	1.292360E 00	1.825280E 00
1.407090E-03	7.830400E-01	1.281400E 00	1.758950E 00
1.489710E-03	8.155000E-01	1.266660E 00	1.689470E 00
1.573740E-03	8.463000E-01	1.246200E 00	1.618400E 00
1.658960E-03	8.747400E-01	1.219780E 00	1.530450E 00
1.744830E-03	9.005000E-01	1.190470E 00	1.452170E 00
1.831480E-03	9.232300E-01	1.160750E 00	1.376220E 00
1.918800E-03	9.427200E-01	1.131090E 00	1.304700E 00
2.006980E-03	9.588900E-01	1.102490E 00	1.239490E 00
2.095980E-03	9.717400E-01	1.077350E 00	1.181040E 00
2.186540E-03	9.815300E-01	1.055490E 00	1.132960E 00
2.279110E-03	9.886900E-01	1.037520E 00	1.093060E 00
2.374370E-03	9.935300E-01	1.023460E 00	1.061970E 00
2.472090E-03	9.965900E-01	1.014100E 00	1.038960E 00
2.576080E-03	9.983400E-01	1.007460E 00	1.022420E 00
2.684150E-03	9.993100E-01	1.003770E 00	1.012480E 00
2.798050E-03	9.997500E-01	1.001450E 00	1.006200E 00
2.918620E-03	9.999200E-01	1.000130E 00	1.002770E 00
3.046420E-03	9.999800E-01	1.000010E 00	1.001040E 00
3.182110E-03	1.000000E 00	1.000150E 00	1.000460E 00
3.326270E-03	1.000000E 00	1.000010E 00	1.000100E 00
3.479490E-03	1.000000E 00	1.000000E 00	1.000020E 00
3.642360E-03	1.000000E 00	1.000000E 00	1.000000E 00
3.815490E-03	1.000000E 00	1.000000E 00	1.000000E 00
3.999520E-03	1.000000E 00	1.000000E 00	1.000000E 00
4.195140E-03	1.000000E 00	1.000000E 00	1.000000E 00
4.403090E-03	1.000000E 00	1.000000E 00	1.000000E 00
4.624140E-03	1.000000E 00	1.000000E 00	1.000000E 00
4.859120E-03	1.000000E 00	1.000000E 00	1.000000E 00
5.108900E-03	1.000000E 00	1.000000E 00	1.000000E 00
5.374420E-03	1.000000E 00	1.000000E 00	1.000000E 00
5.656660E-03	1.000000E 00	1.000000E 00	1.000000E 00
5.956690E-03	1.000000E 00	1.000000E 00	1.000000E 00
6.275620E-03	1.000000E 00	1.000000E 00	1.000000E 00
6.614640E-03	1.000000E 00	1.000000E 00	1.000000E 00

Inviscid Edge Quantities

U_e/V_∞ = 0.93784

W_e/V_∞ = 0.06019

p_e/p_∞ = 6.46340

$T_e/(V_\infty^2/R)$ = 0.02973

Free-Stream Conditions

M_∞ = 7.40 $Re_\infty L$ = 3.0 x 10^6

Wall Temperature Ratio

T_w/T_o = 0.28570

UNCLASSIFIED
Security Classification

DOCUMENT CONTROL DATA - R & D

(Security classification of title, body of abstract and indexing annotation must be entered when the overall report is classified)

1. ORIGINATING ACTIVITY *(Corporate author)* Arnold Engineering Development Center Arnold Air Force Station, Tennessee	2a. REPORT SECURITY CLASSIFICATION UNCLASSIFIED 2b. GROUP N/A

3. REPORT TITLE

THREE-DIMENSIONAL LAMINAR BOUNDARY-LAYER ANALYSIS OF UPWASH PATTERNS AND ENTRAINED VORTEX FORMATION ON SHARP CONES AT ANGLE OF ATTACK

4. DESCRIPTIVE NOTES *(Type of report and inclusive dates)*

Final Report - July 1970 to May 1971

5. AUTHOR(S) *(First name, middle initial, last name)*

John C. Adams, Jr., ARO, Inc.

6. REPORT DATE December 1971	7a. TOTAL NO. OF PAGES 60	7b. NO. OF REFS 54

8a. CONTRACT OR GRANT NO. b. PROJECT NO. c. Program Element 64719F d.	9a. ORIGINATOR'S REPORT NUMBER(S) AEDC-TR-71-215 9b. OTHER REPORT NO(S) *(Any other numbers that may be assigned this report)* ARO-VKF-TR-71-141

10. DISTRIBUTION STATEMENT

Approved for public release; distribution unlimited.

11. SUPPLEMENTARY NOTES Available in DDC	12. SPONSORING MILITARY ACTIVITY Arnold Engineering Development Center, Air Force Systems Command, Arnold AF Station, Tenn. 37389

13. ABSTRACT

Application of three-dimensional inviscid and viscous (laminar boundary layer) analyses for cold wall hypersonic flows over sharp cones at incidence is presented relative to experimental data, showing surface upwash angles and entrained vortex formation leading to crossflow-induced boundary-layer transition. Three-dimensional neutral inviscid stability theory for stationary disturbances is used to calculate the angular orientation of the entrained vortices in the boundary layer while a maximum crossflow Reynolds number concept is applied for correlation of the onset to vortex formation due to crossflow instability. In general, excellent agreement between boundary-layer theory and experiment is obtained relative to surface upwash angles. The inviscid stability theory yields reasonable estimates for the vortex angular orientation while the correlation of distance to onset of vortex formation by a critical maximum crossflow Reynolds number concept is in good agreement with previous investigations on swept cylinders and wings under subsonic and supersonic conditions. The calculated surface upwash angle and maximum crossflow Reynolds number are found to be sensitive to wall temperature effects with the larger values of the angle or crossflow Reynolds number occurring with the hotter wall.

DD FORM 1 NOV 65 1473

UNCLASSIFIED
Security Classification

14. KEY WORDS	LINK A ROLE	LINK A WT	LINK B ROLE	LINK B WT	LINK C ROLE	LINK C WT
boundary layer transition						
conical bodies						
hypersonic flow						
laminar boundary layer						
vortices						